Journal of Geodesy (1996) 70:805–828

Journal of Geodesy

Stability investigations of a discrete downward continuation problem for geoid determination in the Canadian Rocky Mountains

Z. Martinec

Department of Geophysics, Faculty of Mathematics and Physics, Charles University, V Holešovičkách 2, 180 00 Prague 8, Czech Republic

Received 28 April 1995; Accepted 26 June 1996

Abstract

We investigate the stability of a discrete downward continuation problem for geoid determination when the surface gravity observations are harmonically continued from the Earth's surface to the geoid. The discrete form of Poisson's integral is used to set up the system of linear algebraic equations describing the problem. The posedness of the downward continuation problem is then expressed by means of the conditionality of the matrix of a system of linear equations. The eigenvalue analysis of this matrix for a particularly rugged region of the Canadian Rocky Mountains shows that the discrete downward continuation problem is stable once the topographical heights are discretized with a grid step of size 5 arcmin or larger. We derive two simplified criteria for analysing the conditionality of the discrete downward continuation problem. A comparison with the proper eigenvalue analysis shows that these criteria provide a fairly reliable view into the conditionality of the problem.

The compensation of topographical masses is a possible way how to stabilize the problem as the spectral contents of the gravity anomalies of compensated topographical masses may significantly differ from those of the original free-air gravity anomalies. Using surface gravity data from the Canadian Rocky Mountains, we investigate the efficiency of highly idealized compensation models, namely the Airy-Heiskanen model, the Pratt-Hayford model, and Helmert's 2nd condensation technique, to dampen high-frequency oscillations of the free-air gravity anomalies. We show that the Airy-Heiskanen model reduces high-frequencies of the data in the most efficient way, whereas Helmert's 2nd condensation technique in the least efficient way. We have found areas where a high-frequency part of the surface gravity data has been completely removed by adopting the Airy-Heiskanen model which is in contrast to the nearly negligible dampening effect of Helmert's 2nd condensation technique. Hence, for computation of the geoid over the Canadian Rocky Mountains, we recommend the use of the Airy-Heiskanen compensation model to reduce the gravitational effect of topographical masses.

In addition, we propose to solve the discrete downward continuation problem by means of a simple Jacobi's iterative scheme which finds the solution without determining and storing the matrix of a system of equations. By computing the spectral norm of the matrix of a system of equations for the topographical $5' \times 5'$ heights from a region of the Canadian Rocky Mountains, we rigorously show that Jacobi's iterations converge to the solution; that the problem was well posed then ensures that the solution is not contaminated by large roundoff errors. On the other hand, we demonstrate that for a rugged mountainous region of the Rocky Mountains the discrete downward continuation problem becomes ill-conditioned once the grid step size of both the surface observations and the solution is smaller than 1 arcmin. In this case, Jacobi's iterations converge very slowly which prevents their use for searching the solution due to accumulating roundoff errors.

1. Introduction

The problem of downward continuation of the gravity field from the Earth's surface to the geoid arises from the fact that the solution to the boundary value problem for geoid determination is sought in terms of the gravitational potential on the geoid but that the gravity observations are only available on the Earth's surface. Unfortunately, the Earth's surface for continental areas differs significantly from the geoid, and thus the geoid potential parameters must be derived from surface gravity functionals smoothed or damped to some extent. The downward continuation of the gravity field not only from the Earth's surface to the geoid but also

from the satellite or aerial altitudes to the Earth's surface is one of the trickiest problem of physical geodesy since it belongs to the group of ill-posed problems. An extensive list of papers in the geodetic literature during the last three decades documentates this problem quite obviously: Pellinen (1962), Bjerhammar (1962, 1963, 1976, 1987), Heiskanen and Moritz (1967), Sjöberg (1975), Rummel (1979), Moritz (1980), Cruz (1985), Ilk (1987, 1993), Wang (1988, 1990), Engels et al. (1993), Vaníček at al. (1995), among others. Despite some advancements, further efforts would be necessary to solve the unanswered questions related to this problem.

The downward continuation of gravity data is an ill-posed problem in the sense that the results (on the gravitational potential) do not continuously depend on the observations. The consequence is that error – contaminated data together with roundoff errors result in high-frequency oscillations in the solution. To get a stable solution, some regularization approach is to be applied. A common technique of regularization in the context of geoid determination, used, e.g., by Wang (1988, 1990) or Sideris and Forsberg (1990) has been suggested by Molodenskij et al. (1960) and improved by Moritz (1980, Sect.45). In this technique, the Taylor series expansion transforms the gravity anomalies from the Earth's surface to the geoid. The Taylor series expansion is usually approximated by the first term g_1 only (Moritz, 1980, Sect.47). To avoid the problem with the ill-posedness, the term g_1 is not evaluated properly; it is assumed that the gravity anomalies are linearly dependent on topographical heights, and the integration for the term g_1 is taken over topographical heights and not over surface gravity data. However, the linear relationship between free-air gravity anomalies and topographical heights introduced by Pellinen (1962) holds only approximately (Heiskanen and Moritz, 1967, Figure 7-6). The question that remains to be answered is, how large are the errors of geoidal heights due to adopting this approximation?

The downward continuation problem of the gravitational field is governed by Fredholm's integral equation of the 1st kind, symbolically written as

$$Ku = f \ , \tag{1}$$

where K is an integral operator, f is a known function, and function u is to be determined. To regularize the solution of this equation, Schaffrin et al. (1977), Ilk (1987, 1993), or Engels et al. (1993), suggested that Tikhonov's regularization method be applied to eqn.(1), and solve Fredholm's integral equation of the 2nd kind,

$$(K + \alpha L)u = f \ , \tag{2}$$

where L is a regularization operator and α is a regularization parameter. The choice of an optimal regularization operator L and an optimal regularization parameter α is the main problem of Tikhonov's regularization technique. For instance, if L is the identity operator and α is too large, then the error due to regularization will be too large, and the solution will be too smooth. The consequence is that information contained in observations will be lost adequately. On the contrary, if α is chosen too small, then data errors will be amplified too large, and the norm of an approximate solution will be extremely large.

Bjerhammar (1962, 1963, 1976, 1987) was one of the first geodesists to begin to deal with the discrete downward continuation problem by claiming that gravity observations do not cover the Earth's surface continuously, but, in practical applications, they are known in discrete points only. He discretized Poisson's integral postulating that gravity anomalies are harmonic in space between the Earth's surface and a fully embedded sphere. The established system of linear equations was solved for gravity anomalies on the embedded sphere. Cruz (1985) applied his technique, called the Dirac approach, for continuing the surface $2^o \times 2^o$ and $5' \times 5'$ gravity anomalies (from the area of New Mexico) down to the embedded sphere. He demonstrated that iterations of the Dirac approach converge faster than the least-squares collocation method. However, this result does not necessarily mean that the Dirac approach was well-posed in those particular cases.

In Vaníček et al. (1995) we have independently proposed a very similar technique to the Dirac approach for finding the solution of the downward continuation problem occurring in the geoid height determination problem. By removing the gravitational effect of topographical masses from the surface gravity data using Helmert's condensation technique, the gravitational field in space above the geoid becomes harmonic, and the relationship between Helmert's gravity field on the Earth's surface and the geoid is expressed by Poisson's integral. That is why we discretized Poisson's kernel in a regular $5' \times 5'$ grid, for which mean topographical heights and mean surface gravity anomalies were at our disposal, and solved a large system of linear algebraic equations for gravity data selected from the rugged terrain of the Canadian Rocky Mountains. We did not use any kind of regularization other than integral averaging over geographical cells.

In this paper, we are aiming to investigate the stability of the discrete downward continuation problem in a rigorous way. We particularly intend to give an answer to the following problem. An unstable character of the continuous downward continuation problem is stabilized to some extent by a spatial discretization of the solution because a high frequency part of the solution, the determination of which makes the problem unstable, is a priori excluded from the solution. The cut-off frequency is given by the Nyquist frequency associated with a spatial grid step size. The question arises, what is the smallest spatial grid step size for which the solution to the discrete downward continuation problem still has a stable solution?

We will proceed in the following way. We again employ the discretized form of Poisson's integral to set up the system of linear algebraic equations describing the problem. In contrast to Vaníček et al. (1995), we do not modify Poisson's kernel but assume that the contribution of far-zone integration points to the Poisson integral is determined to a sufficient accuracy using one of the existing global gravitational models of the Earth. The eigenvalue spectrum of the matrix of a system of linear equations and the spectral contents of surface gravity anomalies are two items controlling the stability of the discrete downward continuation problem. We will carry out the eigenvalue analysis of the matrix of a system of equations and analyse the extremal eigenvalues to express the conditionality of this matrix. The conditionality of the matrix will depend on the elevation of the Earth's topography above the geoid since the topographical heights enter the Poisson kernel. We will see that there is a principal difficulty in determining the minimum eigenvalue of this matrix since it is related to the spectral norm of the inverse matrix that we will not be able to construct.

The compensation of topographical masses is another possible way how to stabilize the problem as the spectral contents of the gravity anomalies of compensated topographical masses may significantly differ from those of the original free-air gravity anomalies. Using surface observables from the Canadian Rocky Mountains, we will investigate the efficiency of highly idealized compensation models to dampen high-frequency oscillations of the free-air gravity anomalies. The maximum entropy spectrum method will help us to analyze the power spectral contents of the surface gravity observations.

Having analysed the stability of the downward continuation problem, we suggest a simple Jacobi's iterative scheme for solving linear equations. This enables us to find a solution to the problem without storing the matrix of a system of equations which indeed created some problems in our initial attempt (Vaníček et al., 1995). Finally, the convergency of Jacobi's iterations is checked by the spectral norm of the matrix of a linear system of equations which uniquely controls the convergency of the iterations.

2. Formulation of the downward continuation problem for geoid determination

To begin with, let us recall the formulation of Stokes' pseudo-boundary value problem for geoid determination with a higher-order reference gravity field. This problem leads to finding an anomalous gravitational potential $T^{h,\ell}(r,\Omega)$ that satisfies the following linearized boundary-value problem (Martinec and Matyska, 1996; Martinec and Vaníček, 1996)

$$\nabla^2 T^{h,\ell} = 0 \qquad \text{for } r > r_g(\Omega)\,, \tag{3}$$

$$\left.\frac{\partial T^{h,\ell}}{\partial r}\right|_{r_g(\Omega)+H(\Omega)} + \left.\frac{2}{r_g}T^{h,\ell}\right|_{r_g(\Omega)} = -\Delta g^{\ell}\,, \tag{4}$$

$$T^{h,\ell} \sim O\left(\frac{1}{r^{\ell+1}}\right) \qquad r \to \infty\,, \tag{5}$$

where the geoid is described by an angularly dependent function $r = r_g(\Omega)$, (r,Ω) being the geocentric spherical coordinates, i.e., $(r_g(\Omega),\Omega)$ are points lying on the geoid. We will assume that function $r = r_g(\Omega)$ is not known. Function $H = H(\Omega)$ is the height of the Earth's surface above the geoid reckoned along the geocentric radius. Unlike the geocentric radius of the geoid, we will assume that $H(\Omega)$ is a known function. Since we intend to solve the problem of downward continuation of the gravity field from the Earth's surface to the geoid, we shall assume that $H(\Omega) \geq H_{min} > 0$ throughout the paper. Once $H = 0$, the downward continuation problem has a trivial solution.

The superscript 'h' at $T^{h,\ell}$ emphasizes that the potential is harmonic in space outside the geoid, and thus it differs from the traditionally introduced anomalous gravitational potential T (Heiskanen and Moritz, 1967, Sect. 2-13.) which is harmonic in space outside the Earth only. The harmonicity of $T^{h,\ell}$ in space between the geoid and the Earth's surface can be achieved by removing the gravitational effect of topographical masses (masses between the geoid and Earth's surface) from the potential T. More specifically, topographical masses are compensated by an anomalous mass distribution below the geoid, and only the reduced gravitational effect of compensated masses is subtracted from the potential T. This procedure, described in sections 3 and 4, assumes that the density of the topographical masses is known.

Asymptotic condition (5) states (which is also emphasized by the second superscript ℓ at $T^{h,\ell}$) that only a high-frequency part of the gravitational potential $T^{h,\ell}$ is looked for by solving the problem (3)–(5). We thus assume that low-degree components of the gravitational field are prescribed a priori as the reference field. For instance, a satellite gravitational model cut approximately at degree $\ell = 20$ can be taken as the reference. The right-hand sides of the boundary condition (4), gravity anomalies Δg^{ℓ}, are assumed to be given continuously on the Earth's surface. They consist of high-frequency parts of the free-air gravity anomalies, the direct topographical effect on gravity, and the secondary indirect topographical effect on gravity. We refer the reader to Martinec (1993), and Martinec and Vaníček (1994a,b) for definitions and the numerical determination of the two topographical effects.

Two approximations will be imposed on the boundary-value problem (3)–(5). First, we will assume that the radius of the geoid in the anomalous potential $T^{h,\ell}$ may be approximated by a mean radius of the Earth, R,

$$r_g(\Omega) \doteq R\,. \tag{6}$$

This spherical approximation of the geoid guarantees an accuracy better then 1.3×10^{-3}. Since $T^{h,\ell}$ for $\ell > 20$ contributes to geoidal heights by 8 metres at most (Vaníček and Kleusberg, 1987), the error of spherical approximation of the geoid does not exceed the 1 cm level. This approximation is thus admissible in most practical applications and will be used throughout the paper.

Inspecting boundary condition (4), we can see that the term $\partial T^{h,\ell}/\partial r$ is referred to the Earth's surface, whereas term $2T^{h,\ell}/r$ is referred to the geoid. Hence, eqn.(4) represents a non-standard boundary condition with the unknown referred to the two boundaries coupled by height $H(\Omega)$. In fact, there are at least three possibilities with which to treat such an unusual form of the boundary condition. The most common and also the easiest way, used, e.g., by Vaníček and Kleusberg (1987), is based on a belief that the approximation

$$\left.\frac{\partial T^{h,\ell}}{\partial r}\right|_{r_g+H} \doteq \left.\frac{\partial T^{h,\ell}}{\partial r}\right|_{r_g} \tag{7}$$

does not generate large errors in the resulting geoidal heights. The solution to the problem (3)–(5) is then easily found by employing Stokes' integration (Heiskanen and Moritz, 1967, Sect.2-16.). However, Vaníček et al. (1995) show that the approximation (7) may cause systematic errors in geoidal heights in magnitudes of several decimetres.

The second possibility utilizes Poisson's integral for the radial derivatives $\partial T^{h,\ell}/\partial r$ (Heiskanen and Moritz, 1967, eqn. 1.93). A strong singular character of the integral kernel composed from the radial derivative of Poisson's kernel may cause instabilities in the numerical solution for short geoidal wavelengths. To avoid these instabilities and make the problem easier to compute, Poisson's integral is evaluated under the assumption that the gravity anomaly is linearly dependent on topographical heights (Moritz, 1980, Sect.48). This assumption holds only approximately for the Earth's body; an open question concerning the size of errors of this approximation remains to be answered.

Perhaps the least drastic approximation is to refer the second term on the left-hand side of eqn.(4) to the Earth's surface. Formally, boundary condition (4) may be rewritten in the form

$$\left.\frac{\partial T^{h,\ell}}{\partial r}\right|_{r_g+H} + \frac{2}{r_g+H}\left.T^{h,\ell}\right|_{r_g+H} = -\Delta g^{\ell} - DT^{h,\ell} , \tag{8}$$

where

$$DT^{h,\ell} = \frac{2}{r_g}\left.T^{h,\ell}\right|_{r_g} - \frac{2}{r_g+H}\left.T^{h,\ell}\right|_{r_g+H} . \tag{9}$$

Let us make an estimate of the maximum size of $DT^{h,\ell}$,

$$\left|DT^{h,\ell}\right| \doteq \frac{2}{R}\left|\left.\frac{\partial T^{h,\ell}}{\partial r}\right|_{r_g+H}\right| H \leq 200\frac{H}{R}\,\mathrm{mGal} \leq 0.25\,\mathrm{mGal} , \tag{10}$$

where a high frequency part of the gravity disturbances $\partial T^{h,\ell}/\partial r$ on the Earth's surface has been estimated by the value of 100 mGal, and the height H of the Earth's surface above the geoid has been estimated at 8900 metres. In most practical applications, the term $DT^{h,\ell}$ may be neglected because its maximum size is less than the accuracy of the gravity data available for geoid determination. For instance, the accuracy of gravity anomalies available for determination of the gravimetric geoid in the territory of Canada varies from 0.5 mGal to a few milligals (Vaníček, 1995, personal communication). When the accuracy of the gravity anomalies is better than 0.25 mGal, then the term $DT^{h,\ell}$ may be computed from existing models of the geoid, or the problem (3)–(5) may be solved iteratively starting with $DT^{h,\ell}$=0, and improving it successively.

In summary, the problem (3)–(5) may be reformulated in terms of function $\tau^{\ell}(r,\Omega)$,

$$\tau^{\ell}(r,\Omega) = r\frac{\partial T^{h,\ell}}{\partial r} + 2T^{h,\ell} , \tag{11}$$

as

$$\begin{aligned} \nabla^2\tau^{\ell} &= 0 && \text{for } r > R , && (12)\\ \left.\tau^{\ell}\right|_{R+H(\Omega)} &= f(\Omega) , && && (13)\\ \tau^{\ell} &\sim O\left(\frac{1}{r^{\ell+1}}\right) && r \to \infty , && (14) \end{aligned}$$

where the geoid has already been approximated by a mean Earth's sphere, cf. eqn.(6), and $f(\Omega)$ stands for a known 'data' functional prescribed continuously over the Earth's surface. (An explicit form of $f(\Omega)$ is derived in the next two sections.) Our goal is to solve the boundary-value problem (12)–(14) and find function τ^{ℓ} in space outside the geoid. Particularly, we are looking for τ^{ℓ} on the geoid, i.e., $\tau^{\ell}(R,\Omega)$. The last problem is often called the downward continuation of a harmonic function (in our case, function τ^{ℓ}) since a harmonic function is computed on the lower boundary (the geoid) from its value on the upper boundary (the Earth's surface) (Heiskanen and Moritz, 1967, Sect. 8-10.).

3. Idealized compensation models of topographical masses

Now, let us quickly discuss possible ways of compensating the topographical masses for the purpose of geoid computation. Let us begin with Newton's integral for the gravitational potential $V^t(r,\Omega)$ induced by the topographical masses,

$$V^t(r,\Omega) = G\int_{\Omega_0}\int_{r'=R}^{R+H(\Omega')} \frac{\varrho(r',\Omega')}{L(r,\psi,r')} r'^2 dr' d\Omega' , \tag{15}$$

where $\varrho(r,\Omega)$ is the (known) density of topographical masses, and $L(r,\psi,r')$ is the distance between the computation point (r,Ω) and an integration point (r',Ω'),

$$L(r,\psi,r') = \sqrt{r^2 + r'^2 - 2rr'\cos\psi} . \tag{16}$$

It is a well-known fact that the equipotential surfaces of V^t undulate by several hundreds of metres with respect to a level ellipsoid. The fact that undulations of the observed geoid are significantly smaller than those induced by the topographic masses indicates that there must exist a compensation mechanism which reduces the gravitational effect of the topographical masses. This mechanism is probably mainly connected with the lateral mass heterogeneities of the crust, but partly also with deep dynamical processes (Matyska, 1994). To describe the compensation mathematically, a number of more or less idealized compensation models have been proposed. For the purpose of geoid computation, we may, in principle, employ any compensation model generating a harmonic gravitational field outside the geoid. For instance, the topographic-isostatic compensation models are based on compensation by the anomalies of density distribution $\varrho_c(r,\Omega)$ in a layer between the geoid and the compensation level $R - D(\Omega)$, $D(\Omega) > 0$, i.e., the gravitational potential

$$V^{isost.}(r,\Omega) = G\int_{\Omega_0}\int_{r'=R-D(\Omega')}^{R}\frac{\varrho_c(r',\Omega')}{L(r,\psi,r')}r'^2 dr' d\Omega' \ , \tag{17}$$

reduces the gravitational effect of the topographical masses.

In the past, two extremely idealized isostatic compensation models were proposed to cancel the effect of topographical abundances from the surface gravity observations. In the Pratt-Hayford model (e.g., Heiskanen and Moritz, 1967, Sect.3-4.), the topographical masses are compensated by varying the density distribution within the layer of a constant thickness, $D(\Omega) = D_0 = const.$ The compensation density ϱ_c is prescribed as $\varrho_c(\Omega) = \varrho_0 H(\Omega)/D_0$, where $\varrho_0 = 2.67$ g/cm^3 is the mean crustal density. The Airy-Heiskanen model (ibid.) suggests that the topographical masses are compensated by the varying thickness $D(\Omega)$ of the compensation layer. The density of the compensation layer is considered constant equal to the density contrast $\Delta\varrho_{Moho}$ (=const>0) at the Moho discontinuity, i.e., $\varrho_c(\Omega) = \Delta\varrho_{Moho}$, and $D(\Omega) = \varrho_0 H(\Omega)/\Delta\varrho_{Moho}$. The density jump at the Moho discontinuity will be taken according to Martinec (1994), $\Delta\varrho_{Moho}$=0.28 g/cm^3. Both the models assume that the compensation is strictly local and confined to the uppermost regions of the Earth's interior.

In a limiting case of the Pratt-Hayford model, the topographic masses may be compensated by a mass surface located on the geoid, i.e., by a layer whose thickness is infinitely small. This kind of compensation, called the Helmert 2nd condensation (Helmert, 1884), is described by the surface Newton integral:

$$V^{conden.}(r,\Omega) = GR^2\int_{\Omega_0}\frac{\sigma(\Omega')}{L(r,\psi,R)}d\Omega' \ . \tag{18}$$

where $\sigma(\Omega)$ is the density of a condensation layer.

4. The isostatic and Helmert's gravity anomalies

Having introduced a compensation mechanism for the topographical masses, the associated compensation potential V^c approximating the topographical potential V^t reads

$$V^c = V^{isost.} \qquad \text{or} \qquad V^c = V^{conden.} \tag{19}$$

for the respective isostatic compensation and Helmert's 2nd condensation of topographical masses. Martinec (1993) shows that the *residual topographical potential* δV,

$$\delta V = V^t - V^c \ , \tag{20}$$

for both the isostatic compensation and Helmert's 2nd condensation models contributes to the geoidal heights by at most a few metres in mountainous areas.

By means of the residual topographical potential δV, we can write an explicit form of function $f(\Omega)$ introduced on the right-hand side of eqn.(13) (Martinec et al., 1993):

$$f(\Omega) = -[R + H(\Omega)]\left[\Delta g^{F,\ell}(\Omega) + \delta A^{\ell}(\Omega) + \delta S^{\ell}(\Omega)\right] \ , \tag{21}$$

where $\Delta g^{F,\ell}(\Omega)$ is a high-frequency part of the free-air gravity anomaly, $\delta A^{\ell}(\Omega)$ is a high-frequency part of the direct topographical effect on gravity at the Earth's surface, $\delta A(\Omega)$,

$$\delta A(\Omega) = \left.\frac{\partial \delta V(r,\Omega)}{\partial r}\right|_{r=R+H(\Omega)} \ , \tag{22}$$

and $\delta S^{\ell}(\Omega)$ is a high-frequency part of the secondary indirect topographical effect on gravity at the geoid, $\delta S(\Omega)$,

$$\delta S(\Omega) = \frac{2}{R}\delta V(R,\Omega) \ . \tag{23}$$

The formulae suitable for calculating the topographical effects $\delta A(\Omega)$ and $\delta S(\Omega)$ are presented in detail in Martinec (1993) and Martinec and Vaníček (1994a,b).

5. Poisson's integral

Let us turn our attention to the external Dirichlet's problem for the Laplace equation,

$$\nabla^2\tau^{\ell} = 0 \qquad \text{for } r > R \ , \tag{24}$$

$$\tau^{\ell}\big|_R = g(\Omega) \ , \tag{25}$$

$$\tau^{\ell} \sim O\left(\frac{1}{r^{\ell+1}}\right) \qquad r \to \infty \ , \tag{26}$$

where g is a known angularly dependent function. This problem may be thought of as opposite to the problem (12)–(14) since function τ^{ℓ} is looked for outside the geoid ($r = R$) from its values $g(\Omega)$ on the geoid. In the geodetic literature, this problem is called the upward continua-

tion of a harmonic function (Heiskanen and Moritz, 1967, Sect.6-6.).

In contrast to problem (12)–(14), the solution to the upward continuation problem can be found by a simple integration. Writing the harmonic representation of function $\tau^\ell(r,\Omega)$, $r > R$, as

$$\tau^\ell(r,\Omega) = \sum_{j=l}^{\infty}\sum_{m=-j}^{j}\left(\frac{R}{r}\right)^{j+1}\tau^\ell_{jm}Y_{jm}(\Omega)\ , \qquad (27)$$

where $Y_{jm}(\Omega)$ are complex spherical harmonics and τ^ℓ_{jm} are expansion coefficients to be determined, substituting expansion (27) into boundary condition (25), and employing the orthonormality property of spherical harmonics, we get

$$\tau^\ell_{jm} = \int_{\Omega_0} g(\Omega)Y^*_{jm}(\Omega)d\Omega\ , \qquad (28)$$

where Ω_0 is the full solid angle and the asterisk denotes a complex conjugation. By coefficients τ^ℓ_{jm} and the addition theorem for spherical harmonics (e.g., Edmonds, 1960, Sect.4.6.), the solution to the upward continuation problem may be expressed in terms of the well-known Poisson's integral (Kellogg, 1929, Sect. IX.4)

$$\tau^\ell(r,\Omega) = \frac{1}{4\pi}\int_{\Omega_0}\tau^\ell(R,\Omega')K^\ell(r,\psi,R)d\Omega' \qquad (29)$$

with the kernel

$$K^\ell(r,\psi,R) = \sum_{j=\ell}^{\infty}(2j+1)\left(\frac{R}{r}\right)^{j+1}P_j(\cos\psi)\ , \qquad (30)$$

where ψ is the angular distance between the geocentric directions Ω and Ω', and $P_j(\cos\psi)$ is the Legendre polynomial of degree j. Using the analogy of terminology introduced for Stokes' functions (Vaníček and Kleusberg, 1987), we will call $K^\ell(r,\psi,R)$ the spheroidal Poisson's kernel. This can easily be expressed by means of the (full) Poisson kernel $K(r,\psi,R)$ as

$$K^\ell(r,\psi,R) = K(r,\psi,R) - \sum_{j=0}^{\ell-1}(2j+1)\left(\frac{R}{r}\right)^{j+1}P_j(\cos\psi)\ , \qquad (31)$$

where (Heiskanen and Moritz, 1967, Sect. 1-16.)

$$K(r,\psi,R) = R\,\frac{r^2-R^2}{L^3(r,\psi,R)}\ , \qquad (32)$$

and $L(r,\psi,R)$ stands for the spatial distance between points (r,Ω) and (R,Ω').

The integration in Poisson's integral (29) is to be taken over the full solid angle. For regional geoid determination, it is advantageous to divide the integration domain Ω_0 into near- and far-zone integration subdomains. The near-zone subdomain is created by a spherical cap (of a small radius ψ_0) surrounding the computation point, while the rest of the full solid angle forms the far-zone subdomain. The radius ψ_0 of the near-zone spherical cap may be chosen in various ways; one choice is introduced in Appendix A by eqn.(A5). In Appendix B, we derive the contributions of particular integration sub-domains to Poisson's integral (29). Schematically, Poisson's integral (29) may be written as the sum of three terms having different origins,

$$\tau^\ell(r,\Omega) = \tau^\ell_0(r,\Omega) + \tau^\ell_{\psi_0}(r,\Omega) + \tau^\ell_{\pi-\psi_0}(r,\Omega)\ , \qquad (33)$$

where $\tau^\ell_0(r,\Omega)$ expresses the contribution to Poisson's integral from the integration point being on the same geocentric radius as the computation point, eqn.(B16), $\tau^\ell_{\psi_0}(r,\Omega)$ expresses the contributions of integration points lying within the near-zone spherical cap of radius ψ_0 (except the point $\Omega' = \Omega$), eqn.(B8), and $\tau^\ell_{\pi-\psi_0}(r,\Omega)$ expresses the contribution of far-zone integration points, eqn.(B28). As a matter of fact, Poisson's kernel $K^\ell(r,\psi,R)$ decreases rapidly with growing angular distance ψ. The dominant behaviour of Poisson's kernel in the vicinity of point $\psi = 0$ implies that $\tau^\ell_0(r,\Omega)$ and $\tau^\ell_{\psi_0}(r,\Omega)$ reach much larger values than $\tau^\ell_{\pi-\psi_0}(r,\Omega)$. For instance, in the Canadian Rocky Mountains, $\tau^\ell_0(r,\Omega)$ and $\tau^\ell_{\psi_0}(r,\Omega)$ reach several tens of milligals, while $\tau^\ell_{\pi-\psi_0}(r,\Omega)$ reaches only a few hundreds of microgals (Vaníček et al., 1995). Later on, this fact will be utilized to exclude the far-zone contribution $\tau^\ell_{\pi-\psi_0}(r,\Omega)$ from unknowns to be determined; $\tau^\ell_{\pi-\psi_0}(r,\Omega)$ will be determined by using existing global models of the gravitational potential.

6. A continuous downward continuation problem

Using the Poisson integral (29), the downward continuation problem (12)–(14) means to find function $\tau^\ell(R,\Omega)$ satisfying Fredholm's integral equation of the 1st kind,

$$\boxed{\frac{1}{4\pi}\int_{\Omega_0}\tau^\ell(R,\Omega')K^\ell(R+H(\Omega),\psi,R)d\Omega' = f(\Omega)\ ,} \qquad (34)$$

where known function $H(\Omega) > 0$ is the height of the Earth's surface above the geoid reckoned along the geocentric radius. (Note that once $H(\Omega) = 0$ in a particular direction Ω, the Poisson kernel becomes the Dirac delta function, and eqn.(34) has a simple solution $\tau^\ell(R,\Omega) = f(\Omega)$.)

The solution of the integral eqn.(34) can be expressed in terms of the complete normalized system of eigenfunctions $\{u_i(\Omega)\}$, $\{v_i(\Omega')\}$, and the eigenvalues $\{\lambda_i\}$ of Poisson's kernel. The eigenvalue expansion of $K^\ell(R+H(\Omega),\psi,R)$ can be written as the following infinite sum

$$K^\ell(R+H(\Omega),\psi,R) = \sum_{i=1}^{\infty}u_i(\Omega)\lambda_i v_i^*(\Omega'), \qquad (35)$$

where the asterisk denotes a complex conjugation. The solution of eqn.(34) then reads

$$\tau^\ell(R,\Omega') = \sum_{i=1}^{\infty} \frac{f_i}{\lambda_i} v_i(\Omega') \ , \tag{36}$$

where f_i are the Fourier coefficients of the expansion of $f(\Omega)$ by means of $u_i(\Omega)$, i.e.,

$$f(\Omega) = \sum_{i=1}^{\infty} f_i u_i(\Omega) \ . \tag{37}$$

Numbering λ_i such that they create a non-increasing series, $\lambda_1 \geq \lambda_2 \geq ...$, eigenvalues λ_i of Poisson's kernel are non-negative and approach zero when $i \to \infty$,

$$\lambda_i \geq 0 \ , \qquad \lim_{i\to\infty} \lambda_i = 0 \ . \tag{38}$$

For instance, if $H(\Omega) = H_0 = const. > 0$ all over the full solid angle Ω_0, then

$$\lambda_i = \left(\frac{R}{R+H_0}\right)^{i+1} \ , \tag{39}$$

and $u_i(\Omega)$, $v_i(\Omega')$ are complex fully normalized spherical harmonics.

The series on the right-hand side of eqn.(36) converges (and, thus, represents the solution of eqn.(34)), if and only if the Picard condition holds (Groetsch, 1984, Sect. 1.2; Kondo, 1991, Sect. 6.9; Hansen, 1992):

$$\boxed{\sum_{i=1}^{\infty} \left(\frac{f_i}{\lambda_i}\right)^2 < \infty \ .} \tag{40}$$

The Picard condition says that starting from some point in the summation in eqn.(40), the absolute value of Fourier coefficients f_i must decay faster than the corresponding eigenvalues λ_i.

7. Discretization

So far, the downward continuation problem has been formulated in a continuous way. This means that an infinite number of coefficients f_i should be determined from boundary functional $f(\Omega)$ given continuously at all points on the Earth's surface. In practice, however, the boundary functional $f(\Omega)$ is measured at discrete points only, and hence, the number of coefficients f_i which can be determined from such discrete data is finite. The infinite series (37) must be truncated at some finite cut-off degree. Such a truncation represents a certain type of regularization because a high frequency part of $\tau^\ell(R,\Omega)$, the determination of which makes the problem unstable, is excluded from the solution. A question arises whether the regularization of the solution by truncation of its high-frequency part is efficient enough to stabilize the solution of Fredholm's integral equation (34). Or, more specifically, up to which cut-off degree is the solution of eqn.(34) still numerically stable. Since truncation in a spectral domain corresponds to a given resolution in a spatial domain, we may also look for the smallest spatial grid step $\Delta\Omega$ for which a discretized form of eqn.(34) still has a stable solution.

To answer the above question, let us rewrite the integral equation (34) in a discrete form and find a discrete solution. Let observations of boundary functional $f(\Omega)$ run over a regular angular grid with grid step $\Delta\Omega = (\Delta\vartheta, \Delta\lambda)$, where $\Delta\vartheta$ and $\Delta\lambda$ are grid steps in latitude and longitude, respectively. Let observations result in a finite set of discrete values $f_i = f(\Omega_i)$, $i = 1, ..., N$. The solution $\tau^\ell(R,\Omega)$ may then be parameterized by discrete values $\tau^\ell(R_i,\Omega_i)$, $i = 1, ..., N$, evaluated over the same angular grid as observations f_i. Poisson's integral on the left-hand side of eqn.(34) can be computed using a numerical quadrature with the nodes coinciding with grid intersections and weights w_i.

Moreover, in order to transform the integral equation (34) into a system of linear algebraic equations, we will use the decomposition of Poisson's integral into three constituents, see eqn.(33). The smallest constituent, the far-zone contribution $\tau^\ell_{\pi-\psi_0}(r,\Omega)$, is assumed to be computed in advance, before solving a discrete problem, and hence, $\tau^\ell_{\pi-\psi_0}(r_i,\Omega_i)$ will appear on the right-hand side of eqn.(34). Such handling of the far-zone contribution is made possible by its small size compared to the near-zone contributions $\tau^\ell_0(r,\Omega)$ and $\tau^\ell_{\psi_0}(r,\Omega)$. An outline of how to compute $\tau^\ell_{\pi-\psi_0}(r_i,\Omega_i)$ employing existing global models of the gravitational field is given in Appendix B after eqn.(B5).

The discrete form of Fredholm's integral equation (34) of the 1st kind then reads

$$\boxed{\sum_{j=1}^{N} A_{ij}\tau^\ell(R,\Omega_j) = f(\Omega_i) - \tau^\ell_{\pi-\psi_0}(r_i,\Omega_i)} \tag{41}$$

for $i = 1, ..., N$, where the diagonal elements of square $N \times N$ matrix A_{ij} are equal to

$$A_{ii} = d^\ell(r_i,\psi_0,R) - \frac{1}{4\pi} \sum_{\substack{j=1 \\ j\neq i}}^{N} w_j K^\ell(r_i,\psi_{ij},R) \ , \tag{42}$$

and $d^\ell(r_i,\psi_0,R)$ is given by eqn.(B17) taken at the i-th grid point. The off-diagonal elements A_{ij}, $i \neq j$, read

$$A_{ij} = \begin{cases} \dfrac{1}{4\pi} w_j K^\ell(r_i,\psi_{ij},R) \ , & \text{if } \psi_{ij} \leq \psi_0, \\ 0 & \text{otherwise .} \end{cases} \tag{43}$$

Furthermore, we have abbreviated notations introducing $r_i = R + H(\Omega_i)$.

The Picard condition (40) for a discrete downward continuation problem becomes

$$\sum_{i=1}^{N} \left(\frac{f_i}{\lambda_i} \right)^2 < \infty \ , \tag{44}$$

where λ_i are the eigenvalues of matrix $\boldsymbol{A}$, and f_i are the Fourier coefficients of the expansion of $f(\Omega)$ with respect to the eigenvector of matrix $\boldsymbol{A}$ (do not change f_i with $f(\Omega_i)$). From a purely mathematical point, the discrete Picard condition (44) is always satisfied, and we need not bother with the stability of the solution. However, the discrete problem suffers from a combination of measurement errors, discretization errors, and roundoff errors, and the solution to the discrete problem may become extremely sensitive to these errors. Hence, in practice, before solving the discrete downward continuation problem, it should be checked whether the Fourier coefficients f_i decay faster on average than the eigenvalues λ_i for high frequencies i.

8. Jacobi's iterations

In our initial investigations (Vaníček et al., 1995), we solved the system of linear algebraic equations (41) iteratively setting up and storing matrix $\boldsymbol{A}$ on a computer hard drive. This resulted in a very large matrix and, consequently, a huge amount of computer memory was required to solve eqns.(41). However, this obstacle may be overcome quite simply by employing Jacobi's (or Ritz's) iteration approach for solving a system of linear algebraic equations (Ralston, 1965, Sect. 9.7-1; Rektorys, 1968, Sect.30.2). The basic idea behind Jacobi's iteration solution is quite simple, as this brief description shows. Let the matrix notation of a system of eqns.(41) be written as

$$\boldsymbol{A}\boldsymbol{x} = \boldsymbol{y} \ , \tag{45}$$

where $\boldsymbol{y}$ is a known vector composed from the right-hand sides of eqns.(41), and $\boldsymbol{x}$ consists of unknowns $\tau^{\ell}(R, \Omega_j)$. Let matrix $\boldsymbol{A}$ be arranged in the form

$$\boldsymbol{A} = \boldsymbol{I} - \boldsymbol{B} \ , \tag{46}$$

where $\boldsymbol{I}$ is the unit matrix of order N. Substituting eqn.(46) into eqn.(45), we arrive at

$$\boldsymbol{x} = \boldsymbol{y} + \boldsymbol{B}\boldsymbol{x} \ . \tag{47}$$

The system of eqns.(47) may be solved iteratively starting with

$$\boldsymbol{x} \equiv \boldsymbol{x}_0 = \boldsymbol{y} \ . \tag{48}$$

At the k-th stage of iteration ($k > 0$) we are carrying out $\boldsymbol{x}_k$ according to equation

$$\boldsymbol{x}_k = \boldsymbol{B}\boldsymbol{x}_{k-1} \ . \tag{49}$$

When $|\boldsymbol{x}_k - \boldsymbol{x}_{k-1}|$ is less than some tolerance ϵ, we can stop iterating. The result of this operation yields the solution of eqn.(45):

$$\boldsymbol{x} = \boldsymbol{y} + \sum_{k=1}^{K} \boldsymbol{x}_k \ , \tag{50}$$

where K is the number of iteration steps.

In the k-th stage of iteration, we have to compute the product $\boldsymbol{B}\boldsymbol{x}_{k-1}$ which is nothing else but a discretized form of Poisson's integral (29) (with a slightly modified kernel for the diagonal elements) applied to $\boldsymbol{x}_{k-1}$. Thus, employing Jacobi's iterative approach there is no necessity to evaluate and store matrix $\boldsymbol{A}$ or $\boldsymbol{B}$ separately, but only Poisson's integral is to be carried out K-times by a method of numerical quadrature. Note that the above Jacobi iterative scheme is a discretized version of the iterative method proposed by Heiskanen and Moritz (1967, p.318).

9. Numerical tests

9.1. Analysis of conditionality

The first problem we will investigate numerically concerns the conditionality of the matrix $\boldsymbol{A}$. Judging from the unstable behaviour of the solution to the continuous downward continuation problem, the matrix $\boldsymbol{A}$ may become fairly ill-conditioned or even singular. In such a case, the solution to the discrete problem would be unstable, and other types of regularization, more powerful than simply cutting the solution at the Nyquist frequency $\pi/\Delta\Omega$, $\Delta\Omega$ being a grid step size, would have to be applied.

To analyse the conditionality of matrix $\boldsymbol{A}$, we will use the eigenvalue decomposition technique. According to this method, matrix $\boldsymbol{A}$ can be decomposed to produce three matrices

$$\boldsymbol{A} = \boldsymbol{U}\boldsymbol{\Lambda}\boldsymbol{V}^T \ , \tag{51}$$

where matrices $\boldsymbol{U}$ and $\boldsymbol{V}$ are column-orthogonal (matrix $\boldsymbol{V}$ is also row-orthogonal), and the diagonal matrix $\boldsymbol{\Lambda}$ consists of eigenvalues λ_i, $i = 1, ..., N$. If any eigenvalue is zero or very small, then the matrix $\boldsymbol{A}$ is singular or near to singular. As usual, we will measure the conditionality of a matrix by the condition number κ, defined as the ratio of the largest of the λ_i's to the smallest of the λ_i's (Wilkinson, 1965, Sect. 2.30):

$$\kappa = |\lambda_{max}|/|\lambda_{min}| \ . \tag{52}$$

A matrix is singular if its condition number is infinite. To make the decision whether a matrix is ill-conditioned, we should compare the reciprocal value of the condition number κ with the machine's floating point precision ϵ (for example, $\epsilon \doteq 10^{-6}$ for single precision), and say that problem is ill-conditioned if $1/\kappa$ multiplied by a constant is comparable or less than the machine precision ϵ. For

the constant one may choose a larger dimension of the matrix, or the square root of this number, or another constant; that starts getting into a hardware-dependent question.

The conditionality of our matrix $\boldsymbol{A}$, eqns.(42)–(43), was studied over an area $3^o \times 6^o$, delimited by latitudes 47°N and 50°N, and by longitudes 242°E and 248°E. This area covers a particularly rugged part of the Canadian Rocky Mountains, which is the Columbia Mountains chain. The mean $5' \times 5'$ topographical heights range from 503 to 2425 metres.

Figure 1 is a plot of eigenvalues λ_i of matrix $\boldsymbol{A}$ ordered according to their size. We can observe that the values decrease smoothly with the condition number $\kappa = 2.05$. This behaviour contrasts to that expected from the stability analysis of the continuous case, namely, matrix $\boldsymbol{A}$ is well-conditioned. Unfortunately, the computation of eigenvalues could not be carried out for a larger area because of the huge computational time and memory demands; the above example consumed nearly 45 hours of total CPU time on an HP-715 workstation with 64 MB of the internal memory.

We shall thus attempt to estimate the extremal eigenvalues. In accordance with Gerschgorin's theorem (Wilkinson 1965, Sect.2.13), it holds

$$\lambda_{max} \leq \max_i \sum_{j=1}^{N} |A_{ij}| \ , \tag{53}$$

and

$$\lambda_{min} \geq \min_i (A_{ii} - \sum_{\substack{j=1 \\ j \neq i}}^{N} |A_{ij}|) \ . \tag{54}$$

These estimates can readily be evaluated in the case that Poisson's integration is taken over the full solid angle Ω_0, and the integration kernel is the full Poisson kernel $K(r, \psi, R)$. In such a case the matrix A_{ij} takes the form

$$A_{ii} = \frac{R}{r_i} - \frac{1}{4\pi} \sum_{\substack{j=1 \\ j \neq i}}^{N} w_j K(r_i, \psi_{ij}, R) \ , \tag{55}$$

$$A_{ij} = \frac{1}{4\pi} w_j K(r_i, \psi_{ij}, R) \ , \qquad \text{if } i \neq j \ . \tag{56}$$

From these equations it immediately follows that

$$\sum_{j=1}^{N} |A_{ij}| = \frac{R}{r_i} \ , \tag{57}$$

and, by eqn.(53), the upper limit of the eigenvalues of matrix $\boldsymbol{A}$ is

$$\boxed{\lambda_{max} < 1 \ ,} \tag{58}$$

since $r_i > R$ for any i. The estimate (58) is in full agreement with the maximum size of eigenvalues of matrix $\boldsymbol{A}$

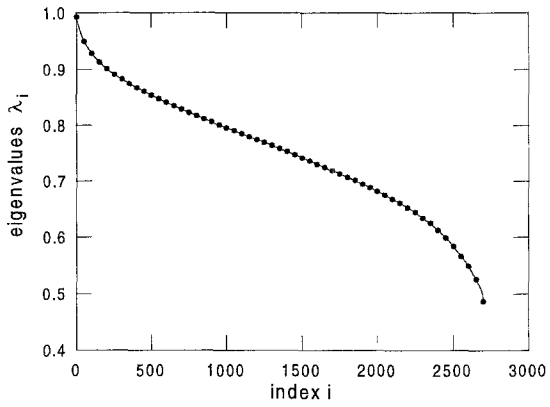

Figure 1: Eigenvalue spectrum of matrix $\boldsymbol{A}$ for the region of Columbia Mountains ($47^o \leq \Phi \leq 50^o$, $242^o \leq \lambda \leq 248^o$) with the $5' \times 5'$ grid of topographical heights.

plotted in Figure 1 because the influence of removing long-wavelength harmonics $j = 0, ..., \ell - 1$, from Poisson's kernel $K(r, \psi, R)$ (in order to create the spheroidal Poisson kernel $K^\ell(r, \psi, R)$) on the largest eigenvalue λ_{max} is tiny. Similarly, the far-zone contribution to Poisson's integral has a very small impact on the property of matrix $\boldsymbol{A}$ (see the discussion after eqn.(33)), and therefore, we can include it in estimates of the extremal eigenvalues of $\boldsymbol{A}$.

To get the lower limit of the eigenvalues λ_i according to eqn.(54), we can proceed as follows:

$$A_{ii} - \sum_{\substack{j=1 \\ j \neq i}}^{N} |A_{ij}| = \frac{R}{r_i} - \frac{1}{2\pi} \sum_{\substack{j=1 \\ j \neq i}}^{N} w_j K(r_i, \psi_{ij}, R) =$$

$$= \frac{R}{r_i} - \frac{1}{2\pi} \int_{\Omega_0 \setminus C_{\psi_1}} K(r_i, \psi, R) d\Omega \ , \tag{59}$$

where spherical cap C_{ψ_1} surrounds the computation point and has the radius which is equal to the minimum of grid step sizes $\Delta\vartheta$ and $\Delta\lambda$. With the help of eqn.(B11), we further have

$$\frac{1}{4\pi} \int_{\Omega_0 \setminus C_{\psi_1}} K(r_i, \psi, R) d\Omega = \frac{R}{r_i} - \frac{r_i + R}{2r_i} \left(1 - \frac{r_i - R}{\ell_i(\psi_1)}\right) \ , \tag{60}$$

where distance $\ell_i(\psi_1)$, given by eqn.(B12), now becomes:

$$\ell_i(\psi_1) = \sqrt{r_i^2 + R^2 - 2 r_i R \cos\psi_1} \ . \tag{61}$$

Substituting eqn.(60) into (59), we get

$$A_{ii} - \sum_{\substack{j=1 \\ j \neq i}}^{N} |A_{ij}| = 1 - \frac{r_i + R}{r_i} \frac{r_i - R}{\ell_i(\psi_1)} \ . \tag{62}$$

Realizing that difference $r_i - R$ is the height H_i of the i-th surface point above the geoid (reckoned along the

geocentric radius), and putting approximately $(r_i+R)/r_i \doteq 2$, we get

$$A_{ii} - \sum_{\substack{j=1 \\ j \neq i}}^{N} |A_{ij}| = 1 - 2\frac{H_i}{\ell_i(\psi_1)} . \qquad (63)$$

In practical applications, ψ_1 is always a small angle. Therefore, we can apply the planar approximation (see Appendix A) to the last term, and write

$$\frac{H_i}{\ell_i(\psi_1)} \approx \frac{H_i}{\sqrt{\ell_0^2(\psi_1) + H_i^2}} = \sin\beta_i , \qquad (64)$$

where

$$\ell_0(\psi_1) = 2R\sin\frac{\psi_1}{2} , \qquad (65)$$

and β_i is the angle between the horizon and the line connecting the i-th point on the Earth's surface with its neighbouring point on the geoid. (Note that β_i is not the angle of inclination of the terrain.) Equation (63) can now be arranged in the form

$$A_{ii} - \sum_{\substack{j=1 \\ j \neq i}}^{N} |A_{ij}| = 1 - 2\sin\beta_i . \qquad (66)$$

To get the lower limit of eigenvalues of matrix $\boldsymbol{A}$, we have to take the minimum of the expression standing on the right-hand side of eqn.(66), i.e.,

$$\lambda_{min} \geq \min_i(1 - 2\sin\beta_i) , \qquad (67)$$

or equivalently,

$$\boxed{\lambda_{min} \geq 1 - 2\max_i(\sin\beta_i) .} \qquad (68)$$

The last inequality is very helpful for estimating the condition number κ of matrix $\boldsymbol{A}$ in the case when $\max_i(\sin\beta_i) < 1/2$, i.e., when $\max_i(\beta_i) < 30^o$. Then, inequality (68) estimates the minimum eigenvalue by a positive number, and we can see whether λ_{min} approaches zero or not, i.e., whether the condition number κ significantly grows or not. Unfortunately, the criterion (68) is of little use once $\beta_i > 30^o$. Then, λ_{min} is estimated by a negative number, and we cannot decide whether λ_{min} is close to zero or not.

Applying estimate (68) to our example shown in Figure 1, we have

$$\sin\beta_i \leq \frac{2.425}{\sqrt{(2 \times 6371 \times \sin 2.5' \times \cos 50^o)^2 + (2.425)^2}}$$

$$\doteq 0.377 , \qquad (69)$$

where 2.425 is the maximum topographical heights (in kilometres) in this region, 6371 is the mean radius of the Earth (in kilometres), $2.5'$ is a half of the discretization step, 50^o is the latitude of the most northern terrain profile. By means of eqn.(68), we have

$$\lambda_{min} > 0.245 . \qquad (70)$$

This estimate is in full agreement with the minimum size of eigenvalues of matrix $\boldsymbol{A}$ plotted in Figure 1 since $\lambda_{min} \doteq 0.48$.

Next, we now attempt to provide another estimate of the condition number by analysing the stability of the solution to the discrete downward continuation problem for a model with constant topographical heights, $H(\Omega) = H_0 = const.$ all over the world (see sect. 6). Assuming that data functional $f(\Omega)$ is given only in discrete points of a regular angular grid with grid step size $\Delta\Omega$, its spectral alias-free series is finite, truncated at degree j_{max}

$$f(\Omega) = \sum_{j=0}^{j_{max}} \sum_{m=-j}^{j} f_{jm} Y_{jm}(\Omega) , \qquad (71)$$

where f_{jm} are expansion coefficients, and $j_{max} < \pi/\Delta\Omega$, where $\pi/\Delta\Omega$ being the Nyquist frequency (e.g., Colombo, 1981). The solution to the discrete downward continuation problem for our simple model of a constant height now reads (see eqn.(36)),

$$\tau^{\ell}(R,\Omega) = \sum_{j=\ell}^{j_{max}} \sum_{m=-j}^{j} \left(\frac{R+H_0}{R}\right)^{j+1} f_{jm} Y_{jm}(\Omega) . \qquad (72)$$

Hence, $\tau^{\ell}(R,\Omega)$ becomes unstable once

$$\left(\frac{R+H_0}{R}\right)^{j_{max}+1} \approx \frac{1}{\epsilon} , \qquad (73)$$

or equivalently,

$$\left(\frac{R+H_0}{R}\right)^{\pi/\Delta\Omega} \approx \frac{1}{\epsilon} , \qquad (74)$$

where ϵ is a machine floating point precision or a constant chosen according to the remark after eqn.(52). Thus, the condition number κ in this particular case can simply be estimated as

$$\kappa \approx \left(\frac{R+H_0}{R}\right)^{\pi/\Delta\Omega} . \qquad (75)$$

In the case when H is not constant over the region under study, we can replace H_0 by the maximum topographical heights H_{max}. Then, such an estimate obviously overestimates the actual condition number, i.e., it is too pessimistic, and hence it holds

$$\boxed{\kappa \leq \left(\frac{R+H_{max}}{R}\right)^{\pi/\Delta\Omega} .} \qquad (76)$$

For the example in Figure 1, we have

$$\kappa \leq \left(\frac{6371+2.425}{6371}\right)^{180\times 12} \doteq 2.28 \ . \qquad (77)$$

We have already learned that the actual condition number is $\kappa = 2.05$, so that criterion (76) estimates κ fairly well. Let us consider another example and put the machine floating point precision $\epsilon = 10^{-6}$ (a single precision), and height $H_0 = 6$ km. Then estimate (76) indicates that the problem is unstable as soon as a discretization step is smaller than $\Delta\Omega \doteq 50$ arcsec.

Summing up, the numerical example shown in Figure 1 demonstrates that cutting the solution to the downward continuation problem for the gravity field at the frequency prescribed a priori by the discretization step of gravity data and/or topographical heights is a very powerful tool for the regularization of the solution. The discrete downward continuation problem may be well-posed even for very rough terrain such as the Rocky Mountains. Nevertheless, the posedness of the discrete downward continuation problem should be treated separately for each specific case. Making a grid of topographical heights denser and denser, there is a limit of a grid step size expressed by criterion (68) or (76) on the conditionality of the matrix $\boldsymbol{A}$ which breaks down the stable behaviour of the discrete downward continuation problem and the problem becomes ill-posed. Then some kind of regularization technique outlined in introduction must be applied.

9.2. Analysis of convergency

Now, let us have a look at the convergency of Jacobi's iterations (45)-(50). The necessary and sufficient condition ensuring that Jacobi's iterative method converges is that the maximum eigenvalue of matrix $\boldsymbol{B}$, $\lambda_{max}(\boldsymbol{B})$, is less than 1 (Ralston, 1965, Sect. 9.7-1),

$$\lambda_{max}(\boldsymbol{B}) < 1 \ . \qquad (78)$$

The largest eigenvalue of matrix $\boldsymbol{B}$ can, for instance, be estimated by the Gerschgorin inequality (53). This estimate may be pessimistic yielding $\lambda_{max}(\boldsymbol{B})$ close to 1. That is why we shall determine $\lambda_{max}(\boldsymbol{B})$ precisely by an iterative process called the power method (Ralston, 1965, Sect. 10.2). The idea of this method is simple. Choose a vector $\boldsymbol{v}_0$ such that it has a non-zero component in the direction of the eigenvector associated with the maximum eigenvalue $\lambda_{max}(\boldsymbol{B})$ (if we happen to choose vector $\boldsymbol{v}_0$ perpendicular to the eigenvector associated to the maximum eigenvalue $\lambda_{max}(\boldsymbol{B})$ and the approach does not work, we repeat it starting with a different $\boldsymbol{v}_0$), and generate a set of vectors $\boldsymbol{v}_k$ according to the prescription

$$c_k \boldsymbol{v}_k = \boldsymbol{B}\boldsymbol{v}_{k-1} \ , \qquad (79)$$

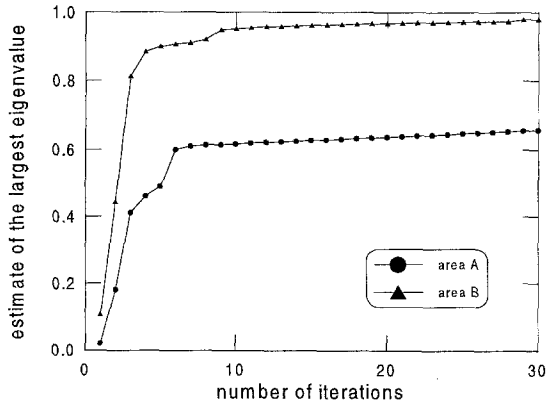

Figure 2: Sequence of numbers c_k, $k = 1, 30$, for our two areas. Figure shows that the limit of c_k for $k \to \infty$ is approximately equal to 0.67 for area A, and 0.98 for area B.

where c_k is equal to the component of vector $\boldsymbol{B}\boldsymbol{v}_{k-1}$ of the largest size. Numbers c_k then converge to $\lambda_{max}(\boldsymbol{B})$,

$$\lim_{k\to\infty} c_k = \lambda_{max}(\boldsymbol{B}) \ . \qquad (80)$$

In the k-th stage of iteration, we only need to compute vector $\boldsymbol{B}\boldsymbol{v}_k$ and not matrix $\boldsymbol{B}$ separately. Again, as in the case of Jacobi's iterative approach, this leads to us carrying out a discretized Poisson integral (29) by a method of numerical quadrature.

The maximum eigenvalue of matrix $\boldsymbol{B}$ has been determined for two areas. In area A, delimited by latitudes 40°N and 76° N, and by longitudes 214°E and 258°E which covers the whole region of the Canadian Rocky Mountains, the topographical heights are sampled as means in 5′ by 5′ grid. The height ranges from 0 to 3993 metres. The topographical heights in area B, delimited by latitudes 47°N and 57°N, and longitudes 238°E and 248°, are gridded much denser (30″ by 60″) than in area A. The height ranges from 0 to 3573 metres. This area covers a particularly rugged part of the Canadian Rocky Mountains, the Columbia Mountains chain.

Figure 2 shows the result of iterations (79), i.e., the sequence of numbers c_k, $k = 1, ...30$. The limit of c_k's yielding $\lambda_{max}(\boldsymbol{B})$ is approximately equal to 0.67 for area A, and 0.98 for area B. The Jacobi iterative scheme will undoubtedly converge in the case of area A, while for area B, with a very dense grid of topographical heights, Jacobi's iterations will converge very slowly since the maximum eigenvalue is very close to 1. Let us have a look at the condition number κ of matrix $\boldsymbol{A}$ for area B. Criterion (68) yields

$$\lambda_{min} > 1 - 2\frac{3.573}{\sqrt{(2\times 6371\times \sin 30'' \times \cos 57°)^2 + (3.573)^2}}$$

$$\doteq -0.925 \ , \qquad (81)$$

where 3.573 is the maximum topographical heights (in kilometres) in this region, 6371 is the mean radius of the

Earth (in kilometres), $30''$ is a half of the discretization step in longitude direction, 57^o is the latitude of the northernmost terrain profile. This is the case when the criterion (68) cannot help us to estimate the condition number κ since we cannot decide how close λ_{min} is to zero. Let us attempt to use criterion (76); for area B it reads

$$\kappa \leq \left(\frac{6371+3.573}{6371}\right)^{180\times 120} \doteq 1.9\times 10^5 \ . \qquad (82)$$

(Note that this criterion gives $\kappa \leq 3.87$(!) for area A.) Since 1.9×10^5 begins to approach the reciprocal value of machine floating point precision (for arithmetic operations in single precision), the downward continuation problem for area B is ill-posed. Searching the solution to the discrete downward continuation problem for area B by Jacobi's iterative scheme, we can run into serious difficulties connected with accumulating roundoff errors (Ralston, 1965, Sect. 9.7-3).

9.3. Power spectrum analysis of gravity anomalies

For regional geoid computation, the downward continuation problem should be solved over as large an area as possible in order to minimize the margin effect of truncated Poisson's integration (Vaníček et al., 1995). The discretization of the problem then leads to a matrix of huge dimensions, and, unfortunately, present-day computers are not able to carry out the eigenvalue analysis. Thus, at present, we cannot check directly the validity of the Picard condition (44) for a discrete downward continuation problem in geoid computation.

Nevertheless, we can ask about the spectral property of function $f(\Omega)$. Equation (21) shows that function $f(\Omega)$, and hence also its Fourier coefficients f_i, depends on the method of compensation of topographical masses. For the purpose of geoid computation, we may, in principal, employ any compensation model the gravitational field of which is harmonic in the space outside the geoid. Thus, we may ask which model of the compensation of topographical masses reduces a high-frequency part of $f(\Omega)$ most efficiently? Such a model will be most convenient one for solving the problem of downward continuation of gravity in geoid height computation because the discrete Picard condition (44) will be satisfied in the best possible way.

As a matter of fact, by a suitable choice of the mass density of a compensation model, we can, in principle, achieve that function $f(\Omega)$ is identically equal to zero (Moritz, 1990, Sect.8.3),

$$f(\Omega) \equiv 0 \ . \qquad (83)$$

The compensation density of such a model is looked for by the deconvolution technique leading to the necessity to solve a system of linear algebraic equation for the parameters of compensation density. We again run into the same problem as above, namely, having to solve a huge system of linear algebraic equations, particularly when a discretization step of $f(\Omega)$ is tiny. We will thus not attempt to construct an 'ideal' compensation density, ensuring that eqn.(83) holds, but we will study the influence of some idealized compensation models with an easily constructed compensation density on the spectral property of function $f(\Omega)$ and attempt to find a compensation model which reduces a high frequency part of $f(\Omega)$ in the most efficient way.

According to the method of isostatic compensation or the condensation of topographical masses (see section 3), function $-f(\Omega)/[R+H(\Omega)]$ will be called the Airy-Heiskanen gravity anomaly, the Pratt-Hayford gravity anomaly, or Helmert's gravity anomaly, respectively. To analyse the spectral contents of the respective gravity anomalies, we have calculated their power spectra by using the autoregressive spectral method, also known as the maximum entropy method (e.g., Marple, 1987, Chapter. 8). The spectral power estimates carried out by this method have a better frequency resolution and increased signal detectability compared to the classical power spectral estimation based on the periodogram. The $5'$ by $5'$ free-air gravity anomaly data and the $5'$ by $5'$ topographical heights (needed for computing the topographical effects) have been considered for the rugged region of the Canadian Rocky Mountains delimited by latitudes $\Phi = 40^o$N and 76^oN, and longitudes $\Lambda = 214^o$E and 258^o (the area A from the preceding section).

In order to show the resulting power spectra as transparent as possible, we have plotted them along chosen longitudinal profiles rather than as isolines or surface plots. Figures 3-6 show the input topographical and free-air gravity data, the Helmert and Airy-Heiskanen gravity anomalies, and corresponding power spectral densities (including the power spectral density of the Pratt-Hayford compensation model) estimated by the maximum entropy method along four longitudinal profiles crossing the Rocky Mountains. Inspecting these figures, and also the power spectra along other profiles (not shown here), we can deduce the following:

- In all the cases we have investigated, the Airy-Heiskanen compensation model reduces high-frequency components of the free-air gravity anomalies in the most efficient way.
- There are profiles (see, e.g., Figure 3 and 4), where Helmert's 2nd condensation technique reduces a short-wavelength part of the free-air gravity anomalies only slightly, while the Airy-Heiskanen model removes this part of the spectra nearly completely.
- We can find the profiles (e.g., Figure 5) along which the Pratt-Hayford model has a similar damping effect on high-frequencies of free-air gravity anomalies as the Airy-Heiskanen model, but there are regions repre-

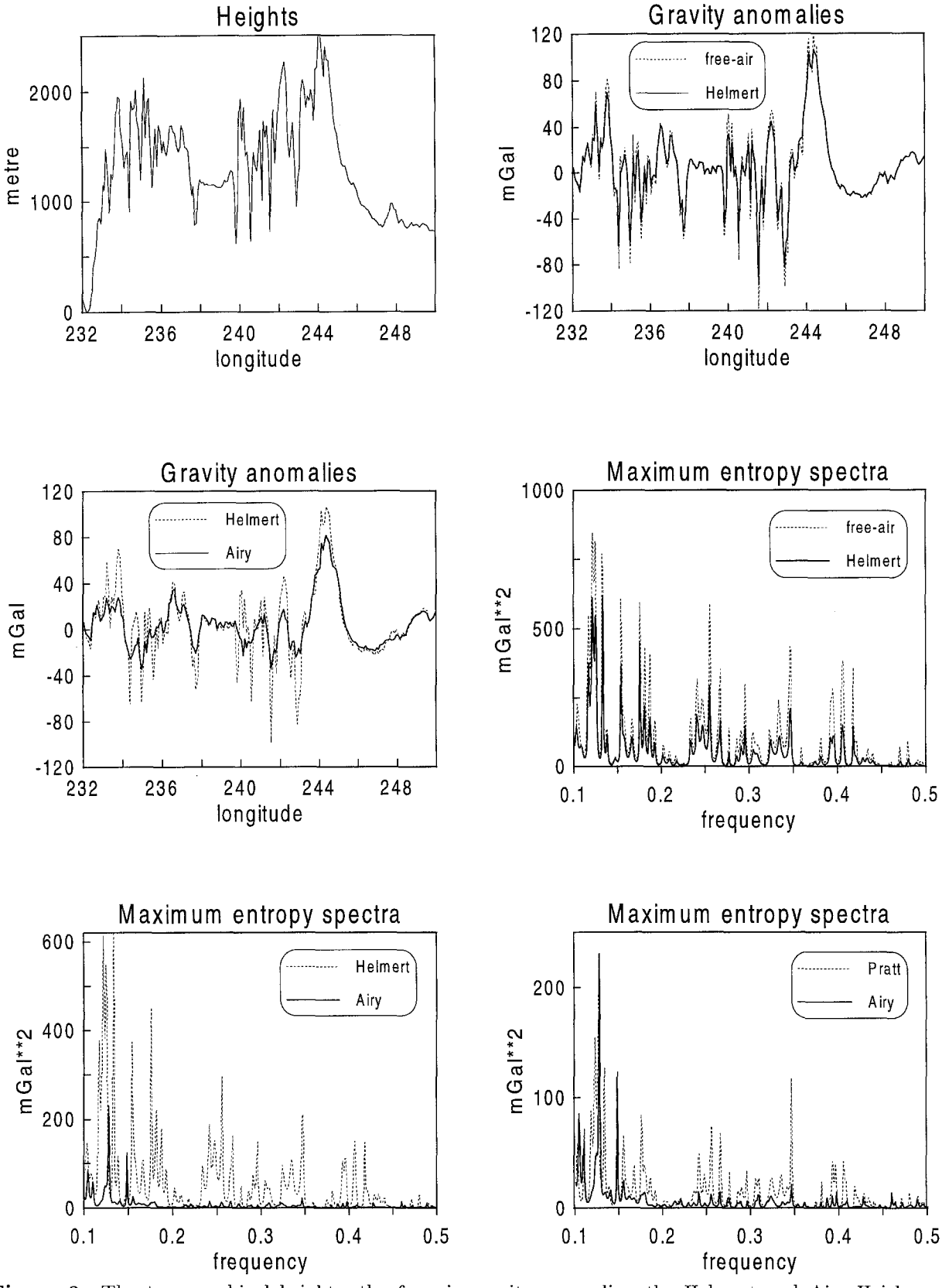

Figure 3: The topographical heights, the free-air gravity anomalies, the Helmert and Airy-Heiskanen gravity anomalies plotted along the longitudinal profile $\Phi = 51.46^{o}$N. The power spectral densities of the respective gravity anomalies (including those of the Pratt-Hayford gravity anomalies) are estimated by the maximum entropy method. The frequency times sampling interval (= 5 arcmin) is drawn on the x-axis of power spectrum figures. Shown is an expanded portion of the full Nyquist frequency interval (which would extend from zero to 0.5).

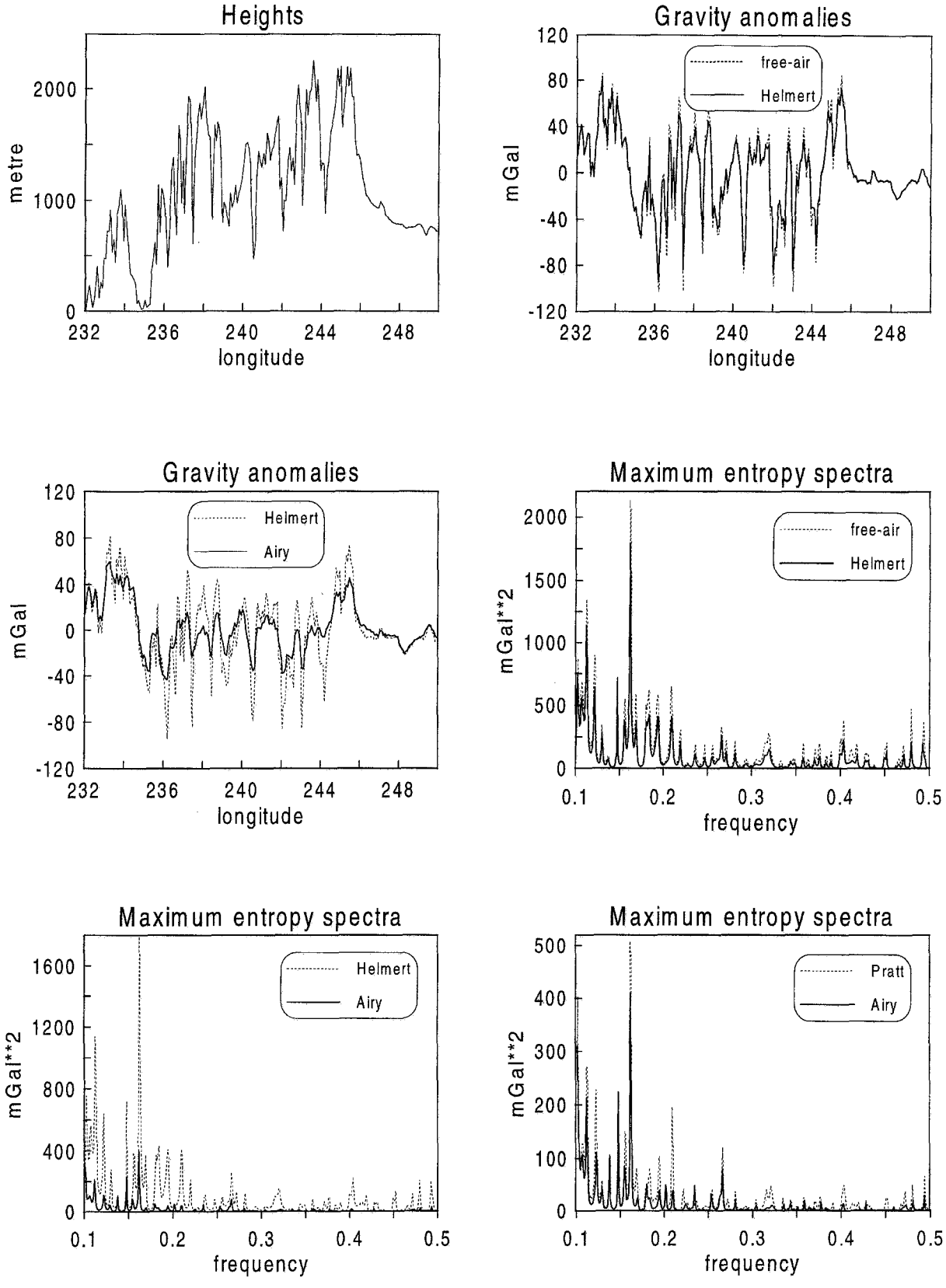

Figure 4: The same as Figure 3 for $\Phi = 50.13^{o}$N.

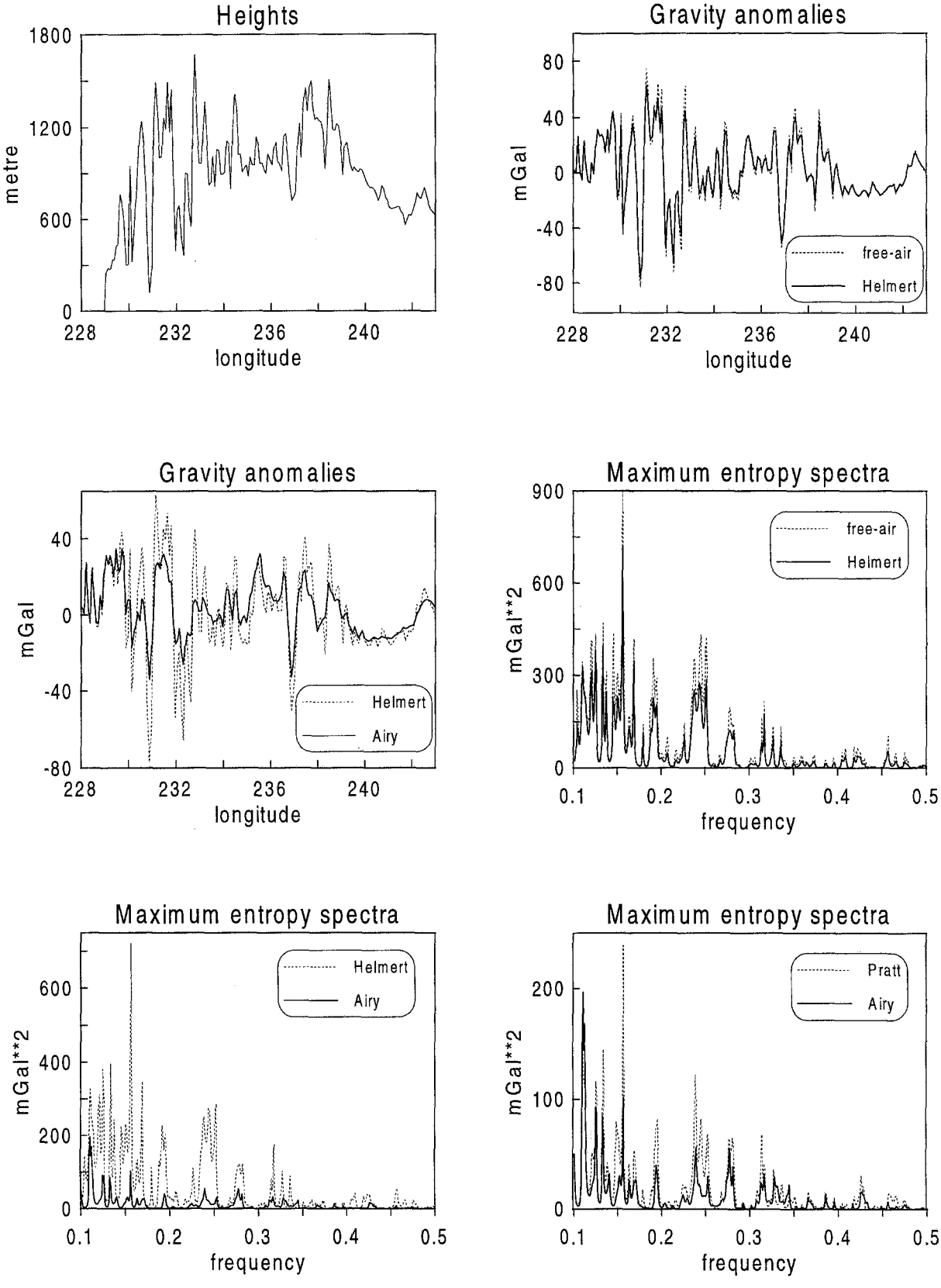

Figure 5: The same as Figure 3 for $\Phi = 55.21°\text{N}$.

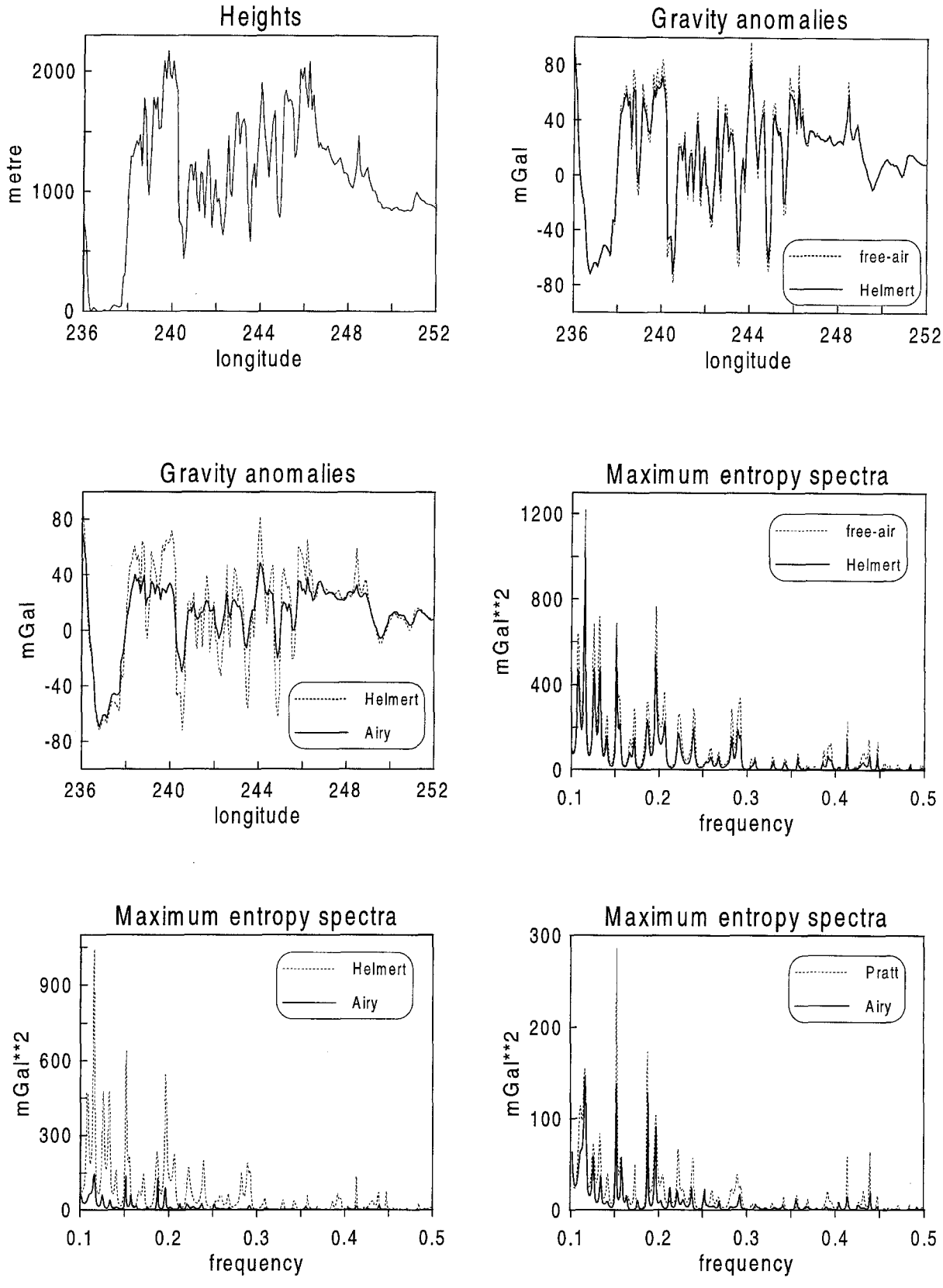

Figure 6: The same as Figure 3 for $\Phi = 48.96°\text{N}$.

sented, for instance, by Figure 6, where the Airy-Heiskanen model reduces short-wavelengths more efficiently than the Pratt-Hayford model.

9.4. Downward continuation of gravity anomalies

Let us finally solve the discretized Fredholm integral equation (41) for the respective surface gravity anomalies, and determine grid values of function $\tau(R, \Omega)$. We use a simple Jacobi's iterative scheme which enables us to find the solution without storing a huge matrix of the system of equations. We have learned that for a region of the Canadian Rocky Mountains with surface observables discretized in a $5' \times 5'$ grid, the matrix of a linear system of equations is well-conditioned (the condition number is equal to 3.9). Moreover, the matrix associated with Jacobi's iterations is contractive with the largest eigenvalue equal to 0.67. These two facts imply that the Jacobi iteration process converges to the solution which is not contaminated by large roundoff errors. To reach the absolute accuracy of the result of about 0.1 mGal, the number of iterations does not exceed 30. The result of this discrete downward continuation procedure will be presented by means of function $D\Delta g(\Omega)$,

$$D\Delta g(\Omega) = \frac{1}{R + H(\Omega)} [\tau(R, \Omega) - f(\Omega)] \ , \qquad (84)$$

which can be understood to be a downward continuation of gravity anomalies.

Figure 7 plots the downward continuation of the Helmert and Airy-Heiskanen gravity anomalies along the four longitudinal profiles shown in Figures 3-6. We can observe that most of the power of $D\Delta g(\Omega)$ is of a very short wavelength. Moreover, as expected from the power spectral analysis, the amplitudes of $D\Delta g(\Omega)$ for the Airy-Heiskanen gravity anomalies are smaller (often significantly smaller) than the corresponding amplitudes of $D\Delta g(\Omega)$ for the Helmert gravity anomalies.

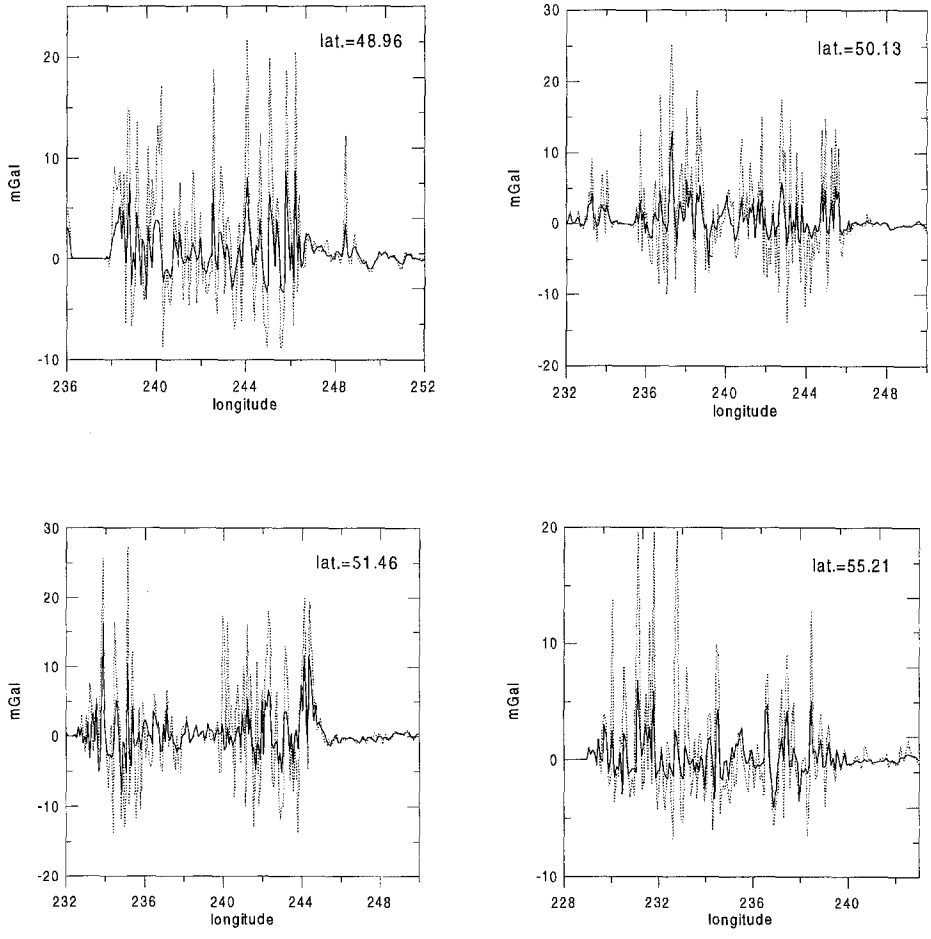

Figure 7: The downward continuation (in milligals) of the Helmert gravity anomalies (dotted lines) and the Airy-Heiskanen gravity anomalies (full lines) along four longitudinal profiles across the Canadian Rocky Mountains.

10. Conclusions

A crucial point of Stokes's method for geoid computation is to continue the gravity observations from the Earth's surface to the geoid. By solving this problem, high-frequency components of the surface gravity data are amplified which may make the problem unstable. The consequence is that error – contaminated data together with roundoff errors result in high frequency oscillations of the solution. This statement drawn for a continuous case is somehow weakened for a discrete downward continuation problem when surface observations are given in discrete points only. Discretizing the solution with the same grid step as the observations then means that a high frequency part of the solution, determination of which makes the problem unstable, is excluded from the solution; the cut-off frequency is given by the Nyquist frequency corresponding to a spatial grid step size.

This paper was motivated by wondering what the smallest grid step size is by which the discretized downward continuation problem is still well-posed. Or alternatively, we looked for the grid step size which surely breaks down the well-posedness of the problem. Note that there is a difference between these two questions since it is not possible to determine a sharp limit between the well-posedness and ill-posedness of a problem. To answer these questions, we have discretized the Poisson integral in a similar fashion to Bjerhammar (1987) or Vaníček at al. (1995), set up the system of linear algebraic equations, and studied the conditionality of the system matrix for the particularly rugged terrain of the Canadian Rocky Mountains.

The only reliable way to treat the conditionality of a matrix is to investigate its eigenvalues and evaluate the ratio of the largest to the smallest eigenvalues. We followed this hint and employed the subroutine SVDCMP (Press et al., 1989) to carry out the eigenvalues of the matrix of a system of equations composed from discretized Poisson's kernel. In spite of this subroutine belonging to the most efficient technique for finding all eigenvalues of a matrix, it has to operate with a full-sized matrix under study. This is a major limitation to its use for exploring the stability of the discrete downward continuation problem because this problem should be solved over as large an area as possible to minimize the margin effect of truncated Poisson's integration (Vaníček et al. 1995). Thus the eigenvalue software package is forced to work with a matrix of huge dimensions, particularly when a discretization step is tiny. On an HP-715 workstation with 64 MB of the memory, we succeeded in carrying out the eigenvalue analysis of the system matrix for an area of $3^o \times 6^o$ with topographical $5' \times 5'$ heights (the dimensions of the matrix to be analysed were 2592×2592). The result of the analysis plotted in Figure 1 is certainly a surprise; the condition number is 2.05 which means that the matrix of a system of linear equations for the discrete downward continuation problem is fairly well-conditioned.

The impossibility of carrying out the eigenvalue analysis for the problem over a larger area with a denser grid step of topographical heights made us propose the simplified criteria (68) and (76) for making a decision whether the matrix $\boldsymbol{A}$ of associated linear algebraic equations is well-conditioned or not. The price paid for their simplicity is that they yield more pessimistic estimates on the conditionality of this matrix than proper eigenvalue analysis. Nevertheless, these criteria provide a fairly reliable estimate on the condition number of matrix $\boldsymbol{A}$ for our test area A. Realizing that the transition between the stability and the instability of the problem is rather broad, the simplified criteria (68) or (76) may give a fairly good view into the stability property and help us to decide whether the discrete downward continuation problem for geoid determination is stable or not.

The second question we dealt with, which is closely related to the posedness of the downward continuation problem, concerned the convergency of Jacobi's iterative scheme suggested for searching the solution to the discrete downward continuation problem. Our analysis of the convergency was based on the fact that the matrix $\boldsymbol{B}$ mediating the iterative solution had to be contractive which means that its largest eigenvalue must be smaller than 1. We used the Gerschgorin estimate (53) of the maximum eigenvalue, but it yielded a pessimistic estimate equal to 1. Therefore, the largest eigenvalue of matrix $\boldsymbol{B}$ was looked for by the power method. As a result, we found that the largest eigenvalue of matrix $\boldsymbol{B}$ is 0.67 for our test area A with topographical $5' \times 5'$ heights. So, we can conclude that Jacobi's iterations will surely converge in this case. Moreover, keeping in mind that the problem is well-posed, the result will not be contaminated by large roundoff errors.

On the other hand, the analysis of the largest eigenvalue of matrix $\boldsymbol{B}$ established for area B with discretization $30'' \times 60''$ shows that Jacobi's iterative scheme will converge very slowly. Using criterion (76) to test the conditionality of matrix $\boldsymbol{A}$, we found that the problem for area B is ill-posed. In such a case, searching the solution by Jacobi's iterative scheme may run into serious difficulties because of the accumulation of the roundoff errors.

Finally, we can answer the two questions posed at the beginning. The discrete downward continuation problem for geoid determination is undoubtedly well-posed and the solution may be looked for by Jacobi's iterative method once the grid step size of the surface observations as well as of the discrete solution is not smaller than 5 arcmin. This conclusion drawn for the Canadian Rocky Mountains will be valid anywhere else in the world, with perhaps the exception of Himalayas, since the Rockies represent one of the highest and most rugged mountainous terrain patterns. On the contrary,

discretizing the same region with grid step size $30'' \times 60''$, we found that the downward continuation problem becomes unstable. In addition, Jacobi's iterations converge very slowly and cannot, in fact, be used for searching the solution.

One possible way to regularize the solution consists of smoothing and dampening high frequency oscillations of the data by compensating the topographical masses in an appropriate way. For a regional geoid computation, present-day computers are, unfortunately, unable to construct an 'ideal' compensation model which would remove completely a high-frequency part of the surface gravity data. We therefore studied the effect of highly idealized compensation and condensation models on the spectral contents of the surface gravity data. We found that for the region of the Canadian Rocky Mountains, the Airy-Heiskanen model reduces a high-frequency part of the gravity data in the most efficient way. On the other hand, we have demonstrated that Helmert's 2nd condensation technique reduces high frequency oscillations in the least efficient way. We found areas ($\Phi = 53^o - 55^o$N, $\Lambda = 231^o - 243^o$E, and $\Phi = 65^o - 66^o$N, $\Lambda = 218^o - 230^o$E) where the Airy-Heiskanen method reduces the high frequency components of surface gravity fairly significantly in contrast to the very small reduction effect of Helmert's 2nd condensation technique. This is surely a consequence of the fact that the latter technique is a pure mathematical tool for the description of compensation of topographical masses, whereas the Airy-Heiskanen model may, in some regions, approximate the actual compensation mechanism fairly well.

So, we recommend that a spectral analysis of the respective gravity anomalies should be carried out before choosing a model of compensation of topographical masses for geoid height computation. Our experience with the spectral analysis and the downward continuation procedure of the gravity observables from the Canadian Rocky Mountains indicates that the Airy-Heiskanen model rather than Helmert's 2nd condensation technique should be used to reduce the high-frequency oscillations of surface gravity data.

Acknowledgements

This work was prepared at the Geodetic Institute of the Stuttgart University where I was stationed as a Fellow of the Alexander von Humboldt Foundation. I would like to thank Prof. E.W. Grafarend for his encouragement to do this study. I am grateful to Prof. P. Vaníček for his continuous interest in the problems related to determination of the accurate geoid. His latest results in this field initiated the research. I wish to thank Dr. M. Véronneau who supplied me with data sets of the digital terrain model of Canada. I wish to express my gratitude to Mrs. G.Fisher and Mr. H.Fisher for the hospitality enjoyed during my stay in their private house. Comments made on the submitted version of the manuscript by two anonymous reviewers have helped to clarify some points and improve the presentation. Ms W. Wells has done an excellent job of correcting the English language of this paper. The research has been partly sponsored by the Grant Agency of the Czech Republic through Grant No. 205/94/0500.

References

Bjerhammar, A. (1962). Gravity reduction to a spherical surface. Report of the Royal Institute of Technology, Geodesy Division, Stockholm.

Bjerhammar, A. (1963). A new theory of gravimetric geodesy. Report of the Royal Institute of Technology, Geodesy Division, Stockholm.

Bjerhammar, A. (1976). A Dirac approach to physical geodesy. *Zeitschrift für Vermessungswesen*, **101**, 41-44.

Bjerhammar, A. (1987). Discrete physical geodesy. Rep. **380**, Dept. of Geodetic Science and Surveying, The Ohio State University, Columbus.

Colombo, O.L. (1981). Numerical methods for harmonic analysis on the sphere. Rep. **310**, Dept. of Geodetic Science and Surveying, The Ohio State University, Columbus.

Cruz, J.Y. (1985). Disturbance vector in space from surface gravity anomalies using complementary models. Rep. **366**, Dept. of Geodetic Science and Surveying, The Ohio State University, Columbus.

Edmonds, A.R. (1960). *Angular Momentum in Quantum Mechanics*. Princeton University Press, Princeton, New Jersey.

Engels, J., E. Grafarend, W. Keller, Z. Martinec, F. Sansò and P.Vaníček (1993). The geoid as an inverse problem to be regularized. In: *Inverse Problems: Principles and Applications in Geophysics, Technology and Medicine*, eds. G.Anger, R.Gorenflo, H.Jochmann, H.Moritz and W.Webers, Akademie-Verlag, Berlin, 122-167.

Groetsch, C.W. (1984). *The Theory of Tikhonov Regularization for Fredholm Equations of the First Kind*. Pitman Publishing, Boston.

Gysen, H. (1994). Thin-plate spline quadrature of geodetic integrals. *Bull. Géod.*, **68**, 173-179.

Hansen, P.C. (1992). Numerical tools for analysis and solution of Fredholm integral equations of the first kind. *Inverse Problems*, **8**, 849-872.

Heiskanen, W.H. and H. Moritz (1967). *Physical Geodesy*. W.H.Freeman and Co., San Francisco.

Helmert, F.R. (1884). *Die mathematischen und physikalischen Theorieen der höheren Geodäsie*, vol.2. Lepzig, B.G.Teubner (reprinted in 1962 by Minerva GMBH, Frankfurt/Main).

Ilk, K.H. (1987). On the regularization of ill-posed problems. In: *Figure and Dynamics of the Earth, Moon, and Planets*, ed. P.Holota, Research Inst. of Geodesy, Topography and Cartography, Prague, 365-383.

Ilk, K.H. (1993). Regularization for high resolution gravity field recovery by future satellite techniques. In: *Inverse Problems: Principles and Applications in Geophysics, Technology and Medicine*, eds. G.Anger, R.Gorenflo, H.Jochmann, H.Moritz and W.Webers, Akademie-Verlag, Berlin, 189-214.

Kellogg, O.D. (1929). *Foundations of Potential Theory.* Berlin, J.Springer (reprinted by Dover Publications, New York,1953).

Kondo, J. (1991). *Integral Equations.* Clarendon Press, Oxford.

Marple, S.L. (1987). *Digital Spectral Analysis with Applications.* Prentice-Hall, Inc., Englewood Cliffs, New Jersey.

Martinec, Z. (1993). Effect of lateral density variations of topographical masses in view of improving geoid model accuracy over Canada. Final report under DSS contract No. 23244-2-4356/01-SS, Geodetic Survey of Canada, Ottawa, June, 1993.

Martinec, Z. (1994). The density contrast at the Mohorovičič discontinuity. *Geophys. J. Int.*, **117**, 539-544.

Martinec, Z. and C. Matyska (1996). On the solvability of the Stokes pseudo-boundary value problem for geoid determination. *J. Geod.*, (in press).

Martinec, Z. and P. Vaníček (1994a). The indirect effect of topography in the Stokes-Helmert technique for a spherical approximation of the geoid. *Man. Geod.*, **19**, 213-219.

Martinec, Z., and P. Vaníček (1994b). Direct topographical effect of Helmert's condensation for a spherical approximation of the geoid. *Man. Geod.*, **19**, 257-268.

Martinec, Z. and P. Vaníček (1996). Formulation of the boundary-value problem for geoid determination with a higher-degree reference field. *Geophys. J. Int.*, **125**, (in press).

Martinec, Z., C. Matyska, E.W.Grafarend and P. Vaníček (1993). On Helmert's 2nd condensation technique. *Man. Geod.*, **18**, 417-421.

Matyska C. (1994). Topographic masses and mass heterogeneities in the upper mantle. *Gravimetry and Space Techniques Applied to Geodynamics and Ocean Dynamics*, Geophysical Monograph **82**, IUGG vol. 17, 125-132.

Molodenskij, M.S., V.F. Eremeev, and M.I.Yurkina (1960). *Methods for Study of the External Gravitational Field and Figure of the Earth.* Translated from Russian by the Israel Program for Scientific Translations for the Office of Technical Services, U.S.Department of Commerce, Washington, D.C., U.S.A., 1962.

Moritz, H. (1980). *Advanced Physical Geodesy.* H.Wichmann Verlag, Karlsruhe.

Moritz, H. (1990). *Figure of the Earth.* H.Wichmann Verlag, Karlsruhe.

Paul, M. (1973). A method of evaluating the truncation error coefficients for geoidal heights. *Bull. Géod.*, **110**, 413-425.

Pellinen, L.P. (1962). Accounting for topography in the calculation of quasigeoidal heights and plumb-line deflections from gravity anomalies. *Bull. Géod.*, **63**, 57-65.

Press, W.H., B.P. Flannery, S.A. Teukolsky, and W.T. Vetterling (1989). *Numerical Recipes. The Art of Scientific Computing.* Cambridge Univ.Press, Cambridge.

Ralston, A. (1965). *A First Course in Numerical Analysis.* McGraw-Hill, Inc., New York.

Rektorys, K. (1968). *Survey of Applicable Mathematics.* SNTL, Prague (in Czech).

Rummel, R. (1979). Determination of short-wavelength components of the gravity field from satellite-to-satellite tracking or satellite gradiometry - An attempt to an identification of problem areas. *Man. Geod.*, **4**, 107-148.

Schaffrin, B., E.D. Heidenreich, and E. Grafarend (1977). A representation of the standard gravity field. *Man. Geod.*, **2**, 135-174.

Shaofeng, and B., D. Xurong (1991). On the singular integration in physical geodesy. *Man. Geod.*, **16**, 283-287.

Sideris, M.G., and R. Forsberg (1990). Review of geoid prediction methods in mountainous regions. *Determination of the Geoid, Present and Future*, Symposium No.106, Milan, June 11-13, 1990, eds. R.H.Rapp and F.Sansò, Springer-Verlag, New York, 1991, 51-62.

Sjöberg, L. (1975). On the discrete boundary value problem of physical geodesy with harmonic reductions to an internal sphere. The Royal Institute of Technology, Stockholm.

Vaníček, P. and A. Kleusberg (1987). The Canadian geoid - Stokesian approach. *Man. Geod.*, **12**, 86-98.

Vaníček, P., W. Sun, P. Ong, Z. Martinec, P. Vajda, and B. Horst (1995). Downward continuation of Helmert's gravity. *Man. Geod.*, (submitted).

Wang, Y.M. (1988). Downward continuation of the free-air gravity anomalies to the ellipsoid using the gradient solution, Poisson's integral and terrain correction - numerical comparison and computations. Rep. **393**, Dept. of Geodetic Science and Surveying, The Ohio State University, Columbus.

Wang, Y.M. (1990). The effect of topography on the determination of the geoid using analytical downward continuation. *Bull. Géod.*, **64**, 231-246.

Wilkinson, J.H. (1965). *The Algebraic Eigenvalue problem.* Clarendon Press, Oxford.

Appendix A. Spherical radius of the near-zone integration cap

In this appendix we will show a possible way to choose the radius of the near-zone integration cap. The idea is based on the effort to express Poisson's kernel in the far-zone domain as a product of the height of the computation point and an isotropic function. Such an expression is suitable for the numerical computation of Poisson's integral over the far-zone domain.

Let us start with the planar approximation of the geoid. The planar approximation of distances (not to be confused with a planar approximation of the geoid), useful for the determination of the regional geoid, is based on the fact that the ratio H/R never exceeds the value of 1.4×10^{-3}. This approximation is admissible because it produces an error of the same order of magnitude as the error of the spherical approximation of the geoid, see eqn.(4). Employing planar approximation of distances, quantities of the order of H/R are neglected with respect to 1. For instance, the planar approximation of the spatial distance $L(R+H, \psi, R)$ between points $(R+H, \Omega)$ and (R, Ω') is simple to derive using eqn.(16):

$$L(R+H, \psi, R) \approx \sqrt{\ell_0^2 + H^2} \ , \qquad (A1)$$

where

$$\ell_0 = 2R \sin \frac{\psi}{2} \qquad (A2)$$

is the (horizontal) spatial distance between points (R, Ω) and (R, Ω').

The radius ψ_0 of a near-zone spherical cap will be chosen such that the spatial distance $L(R+H, \psi, R)$ outside this cap can be approximated by the distance ℓ_0 with an error being not larger than the error of the planar approximation of distances. Writing approximately $L(R+H, \psi, R) \approx \ell_0$ for $\psi > \psi_0$, we make an error of magnitude of H^2/ℓ_0^2. If we require that this error should not be larger than H/R, i.e.,

$$\frac{H^2}{\ell_0^2} \leq \frac{H}{R} \ , \qquad (A3)$$

the radius ψ_0 of the near-zone integration cap is given by the equation

$$\sin \frac{\psi_0}{2} = \frac{1}{2}\sqrt{\frac{H}{R}} \ . \qquad (A4)$$

Since $H/R \ll 1$, we may put $\sin \psi/2 \doteq \psi/2$, and the condition (A4) reduces to:

$$\boxed{\psi_0 = \sqrt{\frac{H}{R}} \ .} \qquad (A5)$$

The near-zone is then defined by those ψ's which are smaller than ψ_0. The smaller the height of the computation point, the smaller the near zone and the larger the far-zone. In the extreme case, when the computational point is on Mount Everest, the near zone extends to the angular distance of about $\psi_0 = 2^o$, and the far-zone from 2^o to 180^o. When $H = 0$, there is no near-zone.

Under the condition (A5), the Poisson kernel $K(r, \psi, R)$, eqn.(32), for integration points lying in the far-zone can be approximated as

$$\boxed{K(r, \psi, R) \doteq \frac{2R^2 H}{\ell_0^3} \qquad \text{for } \psi > \psi_0 \ ,} \qquad (A6)$$

making an error which does not exceed the error of the spherical approximation of the geoid.

Appendix B. Poisson's integration over near- and far-zones

As already introduced for regional geoid determination, it is advantageous to split the integration domain Ω_0 in the Poisson's integral (29) into near- and far-zone subdomains. The near-zone is created by a spherical cap surrounding the computation point, while the rest of the full solid angle creates the far-zone subdomain. The radius ψ_0 of the spherical cap may be chosen in various ways; one possible choice is introduced in Appendix A by eqn.(A5).

Mathematically, splitting the integration domain Ω_0 as

$$\Omega_0 = C_{\psi_0} \cup (\Omega_0 \setminus C_{\psi_0}) \ , \qquad (B1)$$

where C_{ψ_0} is a spherical cap of radius ψ_0, the Poisson integral (29) reads

$$\tau^\ell(r, \Omega) = \overline{\tau}^\ell_{\psi_0}(r, \Omega) + \tau^\ell_{\pi - \psi_0}(r, \Omega) \ , \qquad (B2)$$

where the term

$$\overline{\tau}^\ell_{\psi_0}(r, \Omega) = \frac{1}{4\pi} \int_{C_{\psi_0}} \tau^\ell(R, \Omega') K^\ell(r, \psi, R) d\Omega' \qquad (B3)$$

expresses the contribution of the integration points lying in the near-zone spherical cap, and

$$\tau^\ell_{\pi - \psi_0}(r, \Omega) = \frac{1}{4\pi} \int_{\Omega_0 \setminus C_{\psi_0}} \tau^\ell(R, \Omega') K^\ell(r, \psi, R) d\Omega' \qquad (B4)$$

expresses the contribution of the far-zone integration points. The crucial point lies in the different ways of evaluating the particular contributions to Poisson's integral. The near-zone term $\overline{\tau}^\ell_{\psi_0}(r, \Omega)$ will be evaluated under the assumption that function $\tau^\ell(R, \Omega)$ is given continuously over spherical cap C_{ψ_0}; $\overline{\tau}^\ell_{\psi_0}(r, \Omega)$ will then be determined by computing the integral (B3) using some method of numerical integration. On the contrary, to determine the far-zone contribution $\tau^\ell_{\pi - \psi_0}(r, \Omega)$, we will assume that function $\tau^\ell(R, \Omega)$ is approximated by

a finite spherical harmonic series of the form,

$$\tau^\ell(R,\Omega) = \sum_{j=\ell}^{j_{max}} \sum_{m=-j}^{j} \tau^\ell_{jm} Y_{jm}(\Omega) \ , \qquad (B5)$$

where j_{max} is a finite cut-off degree; $\tau^\ell_{\pi-\psi_0}(r,\Omega)$ will be determined by the summation of a corresponding harmonic series. We thus assume that an estimate of spherical harmonics τ^ℓ_{jm} is available. Inspecting the definition (11) of function τ^ℓ, we can observe that τ^ℓ_{jm}'s may be established by means of the spherical harmonics of potential $T^{h,\ell}$. These harmonics can be set up by employing spherical harmonics of a global gravitational field and spherical harmonics of the Earth's topography; for details we refer the reader to Vaníček et al. (1995), and Martinec and Vaníček (1996).

B.1. Near-zone contribution

To begin with, let us evaluate the near-zone contribution $\overline{\tau}^\ell_{\psi_0}(r,\Omega)$. An increase in magnitude of the spheroidal Poisson kernel $K^\ell(r,\psi,R)$ when $\psi \to 0$ makes the numerical computation of the integral (B3) difficult. There are a variety of techniques on how to compute this integral numerically (e.g., Shaofeng and Xurong, 1991; Gysen, 1994). The most straightforward way is to use the fact that

$$\int_{C_{\psi_0}} K^\ell(r,\psi,R)d\Omega' < \infty \qquad (B6)$$

for $R \neq 0$ and $r \neq 0$, and to remove a small neighbourhood of the point $\psi = 0$ from the integration domain of the integral (B3); the separate contribution of this area is then evaluated analytically. Formally, eqn.(B3) can be written as

$$\overline{\tau}^\ell_{\psi_0}(r,\Omega) = \frac{1}{4\pi}\tau^\ell(R,\Omega)\int_{C_{\psi_0}} K^\ell(r,\psi,R)d\Omega' + \tau^\ell_{\psi_0}(r,\Omega) \ , \qquad (B7)$$

where

$$\tau^\ell_{\psi_0}(r,\Omega) = \\ = \frac{1}{4\pi}\int_{C_{\psi_0}} \left[\tau^\ell(R,\Omega') - \tau^\ell(R,\Omega)\right] K^\ell(r,\psi,R)d\Omega' \ . \qquad (B8)$$

Let us investigate the limit for $\psi \to 0$ of the subintegral function in the angular integral (B8). When $\psi \to 0$, then $\tau^\ell(R,\Omega') \to \tau^\ell(R,\Omega)$. It is reasonable to assume that function $\tau^\ell(R,\Omega)$ is bounded. This assumption means that there are no singularities of the gravitational field above the geoid. As the element $d\Omega'$ of the full solid angle in polar coordinates (ψ,α) is $d\Omega' = \sin\psi d\psi d\alpha$, the limit for $\psi \to 0$ of the subintegral function in eqn.(B8) reads

$$\lim_{\psi\to 0}\left\{\left[\tau^\ell(R,\Omega') - \tau^\ell(R,\Omega)\right] K^\ell(r,\psi,R)\sin\psi\right\} = \\ = \tau^\ell(R,\Omega)\lim_{\psi\to 0}\left[K^\ell(r,\psi,R)\sin\psi\right] - \\ -\tau^\ell(R,\Omega)\lim_{\psi\to 0}\left[K^\ell(r,\psi,R)\sin\psi\right] = 0 \ , \qquad (B9)$$

since we assume throughout the paper that height H of the computation point is only positive, i.e., $H \geq H_{min} > 0$, and thus $K^\ell(R+H,\psi,R) < \infty$ whenever $R > 0$. This also means that $\lim_{\psi\to 0} K^\ell(r,\psi,R) < \infty$, and thus both constituents on the right-hand side of eqn.(B9) are finite.

Let us now evaluate analytically the incomplete angular integral of the spheroidal Poisson kernel occurring in eqn.(B7). As $d\Omega' = \sin\psi d\psi d\alpha$, we have

$$\int_{C_{\psi_0}} K^\ell(r,\psi,R)d\Omega' = \int_{\alpha=0}^{2\pi}\int_{\psi=0}^{\psi_0} K^\ell(r,\psi,R)\sin\psi d\psi d\alpha = \\ = 2\pi\int_{\psi=0}^{\psi_0}\left[K(r,\psi,R) - \right. \\ \left. -\sum_{j=0}^{\ell-1}(2j+1)\left(\frac{R}{r}\right)^{j+1} P_j(\cos\psi)\right]\sin\psi d\psi \ , \qquad (B10)$$

where we have substituted for $K^\ell(r,\psi,R)$ from eqn.(31). The first integral may be evaluated as follows.

$$\int_{\psi=0}^{\psi_0} K(r,\psi,R)\sin\psi d\psi = \\ = R\left(r^2-R^2\right)\int_{\psi=0}^{\psi_0}\frac{\sin\psi d\psi}{\left[r^2+R^2-2rR\cos\psi\right]^{3/2}} = \\ = R\left(r^2-R^2\right)\int_{\cos\psi_0}^{1}\frac{dx}{\left[r^2+R^2-2rRx\right]^{3/2}} = \\ = \frac{r^2-R^2}{r}\left.\frac{1}{\sqrt{r^2+R^2-2rRx}}\right|_{x=\cos\psi_0}^{1} = \\ = \frac{r+R}{r}\left(1-\frac{r-R}{\ell(\psi_0)}\right) \ , \qquad (B11)$$

where

$$\ell(\psi_0) = \sqrt{r^2+R^2-2rR\cos\psi_0} \ . \qquad (B12)$$

In the first step, we have substituted for Poisson's kernel $K(r,\psi,R)$ from eqn.(32) and made the substitution $x = \cos\psi$. Then we have found the primitive function to the indefinite integral over ψ, and, finally, have substituted the lower and upper limit.

The second integral on the right-hand side of eqn.(B10) reads

$$\int_{\psi=0}^{\psi_0}\sum_{j=0}^{\ell-1}(2j+1)\left(\frac{R}{r}\right)^{j+1} P_j(\cos\psi)\sin\psi d\psi = \\ = \frac{R}{r}\int_{\cos\psi_0}^{1} dx + \sum_{j=1}^{\ell-1}(2j+1)\left(\frac{R}{r}\right)^{j+1}\int_{\cos\psi_0}^{1} P_j(x)dx = \\ = \frac{R}{r}(1-\cos\psi_0) - \sum_{j=1}^{\ell-1}(2j+1)\left(\frac{R}{r}\right)^{j+1} R_{j0}(\cos\psi_0) \ , \qquad (B13)$$

where $R_{jk}(x_0)$ stand for the incomplete integrals of the product of two Legendre polynomials (Paul, 1973, eqn. (5)),

$$R_{jk}(x_0) = \int_{-1}^{x_0} P_j(x)P_k(x)dx \ . \qquad (B14)$$

Substituting from eqns.(B10)-(B13) into (B7), we obtain the final form of the near-zone term $\overline{\tau}^{\ell}_{\psi_0}(r,\Omega)$,

$$\overline{\tau}^{\ell}_{\psi_0}(r,\Omega) = \tau^{\ell}_0(r,\Omega) + \tau^{\ell}_{\psi_0}(r,\Omega) \ , \qquad (B15)$$

where

$$\tau^{\ell}_0(r,\Omega) = d^{\ell}(r,\psi_0,R)\tau^{\ell}(R,\Omega) \ . \qquad (B16)$$

The first term on the right-hand side stands for

$$d^{\ell}(r,\psi_0,R) = \frac{1}{2}\left[\frac{r+R}{r}\left(1-\frac{r-R}{\ell(\psi_0)}\right) - \right.$$

$$\left. -\frac{R}{r}(1-\cos\psi_0) + \sum_{j=1}^{\ell-1}(2j+1)\left(\frac{R}{r}\right)^{j+1} R_{j0}(\cos\psi_0)\right] \ , \qquad (B17)$$

and $\tau^{\ell}_{\psi_0}(r,\Omega)$ is given by eqn.(B8).

B.2. Truncation coefficients

Analogous to Molodensky's truncation coefficients for Stokes' function (Heiskanen and Moritz, 1967, Sect. 7-4.), we introduce the truncation coefficients for Poisson's kernel $K(r,\psi,R)$ and spheroidal Poisson's kernel $K^{\ell}(r,\psi,R)$.

Let us introduce an auxiliary function $K^{\psi_0}(r,\psi,R)$ as

$$K^{\psi_0}(r,\psi,R) = \begin{cases} 0 & \text{if } 0 \le \psi < \psi_0 \ , \\ K(r,\psi,R) & \text{if } \psi_0 \le \psi \le \pi \ , \end{cases} \qquad (B18)$$

and expand the function $K^{\psi_0}(r,\psi,R)$ into a series of Legendre polynomials,

$$K^{\psi_0}(r,\psi,R) = \sum_{j=0}^{\infty} \frac{2j+1}{2} q_j(r,\psi_0)P_j(\cos\psi) \ , \qquad (B19)$$

where $q_j(r,\psi_0)$ are expansion coefficients to be determined. Multiplying eqn.(B19) by Legendre polynomial $P_k(\cos\psi)$ and integrating the result over all ψ's, we get

$$\int_{\psi=0}^{\pi} K^{\psi_0}(r,\psi,R)P_k(\cos\psi)\sin\psi d\psi =$$

$$= \sum_{j=0}^{\infty} \frac{2j+1}{2} q_j(r,\psi_0) \int_{\psi=0}^{\pi} P_j(\cos\psi)P_k(\cos\psi)\sin\psi d\psi \ . \qquad (B20)$$

Using the orthogonality property of Legendre polynomials and substituting for $K^{\psi_0}(r,\psi,R)$ from eqn.(B18), the truncation coefficients $q_j(r,\psi_0)$ for Poisson's kernel $K(r,\psi,R)$ read

$$q_j(r,\psi_0) = \int_{\psi_0}^{\pi} K(r,\psi,R)P_j(\cos\psi)\sin\psi d\psi \ . \qquad (B21)$$

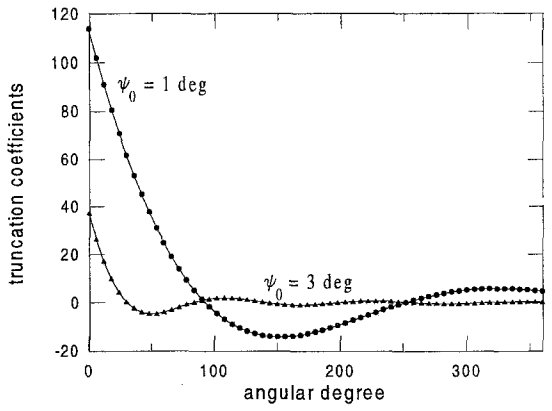

Figure 8: Truncation coefficients $q_j(\psi_0)$ for $\psi_0 = 1^o$ and 3^o, and $j = 0, 1, ..., 360$.

Provided that radius ψ_0 is chosen according to eqn. (A5), the integration in eqn.(B21) is taken over the far-zone domain only. In this case, Poisson's kernel may be approximated by formula (A6), and truncation coefficients $q_j(r,\psi_0)$ become

$$\boxed{q_j(r,\psi_0) \doteq \frac{r-R}{R} q_j(\psi_0) \ ,} \qquad (B22)$$

where

$$\boxed{q_j(\psi_0) = \int_{\psi_0}^{\pi} \frac{1}{4\sin^3\frac{\psi}{2}} P_j(\cos\psi)\sin\psi d\psi \ .} \qquad (B23)$$

For example,

$$q_0(\psi_0) = 2\left(\frac{1}{\sin\frac{\psi_0}{2}} - 1\right) \ . \qquad (B24)$$

To get a rough view into the magnitude of truncation coefficients $q_j(\psi_0)$, Figure 8 plots $q_j(\psi_0)$ for $\psi_0 = 1^o$ and $\psi_0 = 3^o$, and for $j = 0, ..., 360$.

Employing the same procedure as above, we can introduce the truncation coefficients $q^{\ell}_j(\psi_0)$ for the spheroidal Poisson kernel $K^{\ell}(r,\psi,R)$. After some straightforward algebra, we get

$$q^{\ell}_j(r,\psi_0) = \int_{\psi_0}^{\pi} K^{\ell}(r,\psi,R)P_j(\cos\psi)\sin\psi d\psi \ . \qquad (B25)$$

These coefficients can be expressed in terms of truncation coefficients $q_j(r,\psi_0)$ for Poisson's kernel $K(r,\psi,R)$ and Paul's coefficients $R_{jk}(cos\psi_0)$ as

$$\boxed{q^{\ell}_j(r,\psi_0) = q_j(r,\psi_0) - \sum_{k=0}^{\ell-1}\left(\frac{R}{r}\right)^{k+1} R_{jk}(\cos\psi_0) \ .} \qquad (B26)$$

In turn, by means of the truncation coefficients $q^{\ell}_j(r,\psi_0)$, we can express function $K^{\ell,\psi_0}(r,\psi,R)$ which is equal

to $K^{\ell}(r,\psi,R)$ within the interval $\psi_0 \leq \psi \leq \pi$, and vanishes elsewhere, as

$$K^{\ell,\psi_0}(r,\psi,R) = \sum_{j=0}^{\infty} \frac{2j+1}{2} q_j^{\ell}(r,\psi_0) P_j(\cos\psi) \ . \quad (B27)$$

B.3. Far-zone contribution

Now, we are ready to give a spectral form of the far-zone term $\tau^{\ell}_{\pi-\psi_0}(r,\Omega)$. Inserting eqn.(B5) and (B27) into (B4) and interchanging the order of integration and summation, we obtain

$$\tau^{\ell}_{\pi-\psi_0}(r,\Omega) = \frac{1}{2} \sum_{j=\ell}^{j_{max}} q_j^{\ell}(r,\psi_0) \sum_{m=-j}^{j} \tau^{\ell}_{jm} Y_{jm}(\Omega) \ , \quad (B28)$$

where truncation coefficients $q_j^{\ell}(r,\psi_0)$ are given by eqn. (B26).

B.4. Summary

Let us summarize the formulae for the numerical computation of Poisson's integral (29). Schematically, it may be written as a sum of three terms,

$$\boxed{\tau^{\ell}(r,\Omega) = \tau_0^{\ell}(r,\Omega) + \tau^{\ell}_{\psi_0}(r,\Omega) + \tau^{\ell}_{\pi-\psi_0}(r,\Omega) \ ,} \quad (B29)$$

where $\tau_0^{\ell}(r,\Omega)$ expresses the contribution to Poisson's integral from the integration point being on the same geocentric radius as the computation point, eqn.(B16), $\tau^{\ell}_{\psi_0}(r,\Omega)$ expresses the contributions of integration points lying within the near-zone spherical cap of radius ψ_0, eqn.(B8), and $\tau^{\ell}_{\pi-\psi_0}(r,\Omega)$ expresses the contribution of far-zone integration points, eqn.(B28).